Terrestrial, Atmospheric and Oceanic Sciences

RESEARCH **Open Access**

A case study of geoid modeling in Sulawesi and accuracy verification strategies for accommodating diverse MSL vertical datums

Hsuan-Chang Shih[1*], Leni Sophia Heliani[2], Yu-Shen Hsiao[3], Cheinway Hwang[4] and Arisauna Maulidyan Pahlevi[5]

Abstract
This study aims to introduce the geoid modeling process in Sulawesi and demonstrate the practical issues faced. There are limitations of terrestrial gravity surveys in Sulawesi due to its complex geography, so airborne gravity surveys were conducted from 2008 to 2019 through a collaboration between the Badan Informasi Geospasial (BIG), the Technical University of Denmark (DTU), and the National Chiao Tung University (NCTU) gravity research team. The airborne gravity data currently cover almost the entire land area of Indonesia. The geoid modeling process involved refining the EGM08-derived geoid heights by incorporating downward-continued airborne gravity data and RTM-derived geoid effects, and adjusting the geometric geoid heights to accommodate diverse mean sea levels used in different GPS/leveling datasets. The impacts of different global gravitational models (GGMs), such as EIGEN-6C4, GECO, XGM2019e, and SGG-UGM-2, on geoid modeling were examined, and it revealed that differences arise from the different datasets used in the development of the GGM. This study revealed that airborne gravity data can significantly improve the accuracy of the geoid, achieving an impressive accuracy of approximately 0.04 to 0.05 m. In addition, the compatibility issue between gravity data and GGM in geoid modeling is highlighted. The strategy to unify the vertical datum between different GPS/leveling datasets for the validation of gravimetric geoid model was discussed in detail. Once the corresponding geopotential is determined, the conversion between the global vertical datum and the local vertical datum can be achieved. Accurate geoid is critical for infrastructure development, land-use planning, and resource management and play an integral role in supporting sustainable development goals (SDGs) by providing accurate spatial referencing, ensuring precise mapping, and offering location-based services.

Keywords Airborne gravimetry, Geoid modeling, Vertical datum, Indonesia

*Correspondence:
Hsuan-Chang Shih
flex0902@gmail.com
[1]Department of Real Estate and Built Environment, College of Public Affairs, National Taipei University, 151 University Rd., Sanxia Dist, 23741 New Taipei City, Taiwan
[2]Department of Geodetic Engineering, Faculty of Engineering, Universitas Gadjah Mada, Jl Grafika 2, 55281 Yogyakarta, Indonesia
[3]Department of Soil and Water Conservation, National Chung Hsing University, 145 Xingda Rd., South Dist, 402 Taichung City, Taiwan
[4]Department of Civil Engineering, National Yang Ming Chiao Tung University, 1001 Daxue Rd., East Dist, 300093 Hsinchu City, Taiwan
[5]Center for Geodetic Control Networks and Geodynamic, Geospatial Information Agency of Indonesia, Jl. Raya Jakarta - Bogor KM. 46, Kecamatan Cibinong, Kabupaten Bogor, Jawa Barat 16911, Indonesia

1 Introduction

The purpose of the geoid is to define a physically meaningful equipotential surface that can be used as a vertical datum to ensure the continuity of heights across borders, coastline areas, and the globe (Vaníček 1994; Jekeli 2000). One important application of the geoid is to convert ellipsoidal height measured by GNSS into orthometric height. This enables many uses, for example, to convert the ellipsoid heights of airborne lidar point clouds to orthometric heights (Hwang et al. 2020a) and to monitor ocean current dynamics (Hwang et al. 2012) and land subsidence (Vu et al. 2020; Yeh et al. 2025). In addition, the development of a precise geoid model aligns with the United Nations' Sustainable Development Goals (SDGs), specifically Goal 9.A. Goal 9.A emphasizes the development of resilient infrastructure; an accurate geoid is fundamental for engineering projects such as drainage systems and transportation networks by providing a unified vertical datum, which is critical for archipelagic nations like Indonesia. These properties make the geoid particularly suitable for archipelagic countries such as Indonesia. In fact, Indonesia's law on geospatial information No. 4/2011 emphasizes the use of the geoid as a national vertical geospatial reference system (BIG 2022).

To achieve a consistent vertical datum for each island, gravity data covering all regions of Indonesia are needed. Due to Indonesia's extensive territory, numerous islands, and complex terrain, terrestrial gravity data collected since the 1990s do not fully cover the entire nation. To address this challenge, Heliani et al. (2004) proposed a method that combines the gravity values computed by a digital terrain model (DTM) and the gravity anomalies derived from a global gravitational model (GGM) to simulate the terrestrial gravity anomaly field. Additionally, the Badan Informasi Geospasial (BIG) measured 57 absolute gravity points using the A10 absolute gravimeter (Fig. 1). Airborne gravimetry has proven to be a valuable solution to the problem of how to efficiently collect gravity data covering all land areas in Indonesia.

Between 2008 and 2011, a collaboration between the Technical University of Denmark (DTU) and BIG led to airborne gravity surveys in Sulawesi, Kalimantan, and Papua, intending to obtain a geoid for these areas with a target accuracy of 20 cm. Subsequently, from 2018 to 2019, BIG partnered with the National Chiao Tung University (NCTU) gravity research team to conduct airborne gravity surveys in Sumatra, Java, Bali, Nusa Tenggara, and the Moluccas (Pahlevi et al. 2019). As a result, almost all the land areas of Indonesia are now covered by airborne gravity data, marking significant progress in achieving comprehensive gravity coverage, as illustrated in Fig. 1.

The Indonesian geoid, known as 'INAGEOID2020,' was first launched in 2020 (Pahlevi et al. 2024) and was built upon the Earth Geopotential Model 2008 (EGM08) (Pavlis et al. 2012), the DTU17 marine gravity model (Andersen and Knudsen 2019), and gravity datasets in Indonesia (Pahlevi et al. 2019; BIG 2022). The gravity data were derived from terrestrial and airborne gravity measurements. The EGM08, extending up to 2190 degrees, serves as the foundation for determining the geoid in the low-frequency domain. To address the geoid in the high-frequency domain, the fast Fourier transform (FFT) method was employed along with the Space Shuttle Radar Topography Mission (SRTM) v4.1 digital elevation data (Farr et al. 2007), which feature a resolution of 3 arc-second

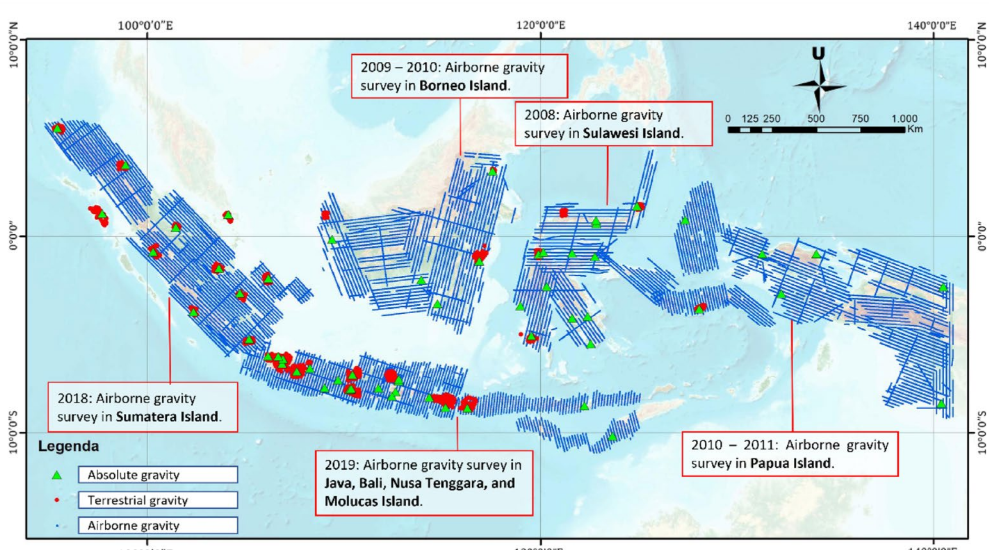

Fig. 1 Distribution of Indonesian absolute, terrestrial and airborne gravity datasets (modified from Hwang et al. 2020b)

(approximately 90 m). A classic remove-compute-restore (RCR) process was further applied to generate the Indonesia geoid model. The accuracy of this geoid model was assessed using GPS/leveling data, resulting in an improvement from the previous version's accuracy at the meter level to the decimeter level. Table 1 outlines the accuracy of the latest geoid models in various regions of Indonesia, including Java, Kalimantan, Bali, Sumatra, and Sulawesi (Pahlevi et al. 2024).

Various aspects of geoid modeling have been presented by the authors in the book compiled by Sansò and Rummel (1997). Wang et al. (2021) provided an overview of geoid modeling methods, focusing on data from the Colorado geoid experiment (Wang et al. 2021). Recent advancements in geoid modeling across the Asia-Pacific region were summarized by Hwang et al., 2021). Geoid modeling relies not only on available gravity data, e.g., GGM, different types of gravity measurements, and DTM-derived gravity estimates but also on geoid modeling approaches. Most of the approaches based on the RCR process, handling the medium- and short-wavelength gravitational signal. The approaches commonly used are based on modified Stokes integration (Sjöberg 2003), the spherical radial basis function (SRBF) (Klees et al. 2008), and least-squares collocation (LSC) (Moritz 1978; Hwang et al. 2007). The DTM-related gravity and geoid computations include techniques based on classical integration (Hwang et al., 2003) and the FFT (Tscherning et al. 1992; Forsberg and Tscherning 2008). The classical integration has better precision than the FFT in areas with complex terrain and similar results in flat areas, while the FFT has faster computation efficiency (Gomez et al. 2013). The resolution and quality of a DTM are other issues that affect gravity and geoid estimates (Grzyb et al. 2006). Since there is no standardization in geoid modeling, the processing flow depends heavily on the available gravity data and the study area. Most of the approaches are based on the GGM, which can characterize the Earth's geoid model except for its zero-degree harmonic. Recent studies represented the contribution of the zero-degree harmonic to the GGM-based geoid and is indispensable for the conversion between global and local vertical datums. (Sánchez et al., 2016; Amin et al. 2019).

Table 1 Accuracy estimates of INAGEOID2020 before fitting the geometric geoid heights to gravimetric geoid model (unit: cm) (Pahlevi et al. 2024)

Island	Standard deviation
Java	12.2
Bali	20.0
Sumatera	29.3
Sulawesi	27.2
West Kalimantan	7.0
East Kalimantan	7.3

In this study, efforts were made to enhance the accuracy of geoid modeling in Sulawesi, where the accuracy of INAGEOID2020 was considered insufficient. The study area spans the longitude range of 118° E- 126° E and the latitude range of 6° S- 6° N. The airborne gravity data covering the land areas of Sulawesi are distributed at an average altitude of approximately 3500 m. The data underwent re-examination to eliminate evident mismatches and biases caused by flight turbulences. The subsequent analysis focused on determining the appropriate degree of the EGM08 for the downward continuation of the airborne gravity data. For geoid modeling, the airborne gravity data were continued down to the surface of the EGM08-derived geoid and utilized to compute its contributions to the geoid, resulting in a more refined geoid model based on the EGM08 and airborne gravity data. Through the contribution of airborne gravity data, the EGM08-derived geoid at a resolution of approximately 9 km (at a degree of 2160) was improved to approximately 5 to 8 km (Hwang et al. 2007; Shih et al. 2015; Ince et al. 2020). A DTM with an 18 arc-second grid spacing sampled from the 'GEBCO_2022' grid was used to calculate the short-scale geoid effects (GEBCO Bathymetric Compilation Group 2022), improving the resolution from ~5 km down to ~500 m (Hirt et al. 2014; Hirt and Rexer 2015; Ince et al. 2020).

The geoid modeling process in this study is as follows: "gravity anomaly > equivalent topography > geoid". The equivalent topography that best matches the gravity anomaly changes is first generated. The technology of fast Fourier transform convolutions in planar approximation (the 2D-FFT technique) was used to calculate the geoid effects of the equivalent topography, based on the 'TCFOUR' program in 'GRAVSOFT' software (Forsberg and Tscherning 2008). The core physical concept is the rapid conversion of the residual gravity anomalies into the residual geoid heights based on the principles of Bouguer's theory and Fourier series expansion. In addition, the EGM08-derived gravity anomalies at 1440, 1800, and 2160 degrees were tested to determine the appropriate degree for geoid modeling. To address the inconsistent mean sea levels (MSLs) used in different GPS/leveling datasets in Sulawesi, the accuracies and relationships between the datasets were studied. All the datasets were then corrected to a consistent datum (as detailed in the section "Estimation of the MSL geopotential") and used to validate the geoid model. Geoid modeling based on different GGMs was evaluated, and the causes of their differences were highlighted. The final geoid model represents a significant improvement in accuracy, offering more precise and reliable geoid information for Sulawesi.

2 Methodology

In this study, the geoid modeling process was developed by using the 2D-FFT technique and the equivalent topography derived from GGM-derived spherical approximated gravity anomalies. The equivalent topographic height H in meters (m) can be calculated as follows:

$$H = \begin{cases} \frac{\Delta g}{2\pi G\rho} \approx \frac{\Delta g}{0.1119} \ if \ \Delta g > 0 \\ \frac{\Delta g}{2\pi G(2670-\rho_0)} \approx \frac{\Delta g}{0.0687} \ if \ \Delta g \leq 0 \end{cases} \quad (1)$$

where $G = 6.67 \times 10^{-11} m^3 kg^{-1} s^{-2}$ is the gravitational constant, $\rho = 2670 \ kg \bullet m^{-3}$ is the standard rock mass density, $\rho_0 = 1030 \ kg \bullet m^{-3}$ is the ocean water mass density and Δg is the GGM-derived gravity anomaly in milligal (mgal).

For determining the geoid height N, one may start from Bruns' formula as follows (Heiskanen and Moritz 1967):

$$N = \frac{T_g}{\gamma_0} - \frac{W_0 - U_0}{\gamma_0} \quad (2)$$

where T_g is the disturbing potential and W_0 is the constant geopotential on the surface of the geoid, whereas U_0 is the normal potential and γ_0 is the normal gravity on the surface of the reference ellipsoid. The geoid aligns the equipotential surface of the constant geopotential W_0 (the geopotential of the geoid). In this study, the normal gravity was computed based on the GRS80 ellipsoid and the constant normal potential $U_0 = 62636860.850 \ m^2 s^{-2}$ (Moritz 2000).

The disturbing potential T_g can be replaced by T^{GGM} to utilize the spherical harmonic coefficients of GGM and the potential of the equivalent topography T^E as follows (Sjöberg and Bagherbandi 2017):

$$T^E = \begin{cases} -2\pi G\rho \left[H^2 + \frac{2H^3}{3R}\right] \ if \ H > 0 \\ 0 \qquad if \ H \leq 0 \end{cases} \quad (3)$$

The disturbing potential T^{GGM} from a set of spherical harmonic coefficient of the GGM can be expressed as

$$T^{GGM} = \frac{GM}{r} \sum_{n=2}^{n} \left(\frac{R}{r}\right)^n \sum_{m=0}^{n} \left(\Delta \bar{C}_{n,m} \cos m\lambda + \Delta \bar{S}_{n,m} \sin m\lambda\right) \bar{P}_{n,m}(\sin\phi) \quad (4)$$

where r, ϕ, λ are spherical radius, spherical latitude and spherical longitude, n, m are spherical harmonic degree and order, GM and R are geocentric gravitational constant and radius of the reference sphere, $\bar{C}_{n,m}$ and $\bar{S}_{n,m}$ are fully normalized spherical harmonic coefficients of degree n and order m, $\bar{P}_{n,m}$ is fully normalized associated Legendre function (Heiskanen and Moritz 1967).

Equation (2) can be rewritten as follows (Sjöberg and Bagherbandi 2017):

$$N = \left(\frac{T^{GGM}}{\gamma_0} + \frac{T^E}{\gamma_0}\right) - \frac{W_0 - U_0}{\gamma_0} = N^{GGM} - \frac{W_0 - U_0}{\gamma_0} \quad (5)$$

where the first term is the GGM-derived geoid height N^{GGM}, including the GGM-derived height anomaly $\frac{T^{GGM}}{\gamma_0}$ and the effect of equivalent topography $\frac{T^E}{\gamma_0}$, and the second term $-\frac{W_0 - U_0}{\gamma_0}$ defines the distance between the constant geopotential W_0 and the normal potential U_0 along the ellipsoidal normal.

The spherical harmonic coefficients of the GGM start from the second degree. The GGM-derived geoid lacks zero- and first-degree terms. The first-degree term was eliminated by selecting the origin of the coordinate system at the Earth's gravity center, and the zero-degree term was given by the second term in Eq. (5), in which the estimation of the geopotential W_0 needs to integrate the geoid heights all over the unit sphere (Sánchez et al., 2016; Amin et al. 2019). On the other hand, the GGM can be expanded by incorporating higher-resolution gravity data. For example, the airborne gravity data contribute to the geoid as N^{AIR}, and the residual terrain model (RTM) derived short-scale geoid is N^{RTM} (Forsberg 1984). The first term in Eq. (5) was replaced by the expanded geoid height N^{GGM+} as follows:

$$N^{GGM+} = N^{GGM} + N^{AIR} + N^{RTM} \quad (6)$$

where N^{AIR} and N^{RTM} can be regarded as the expansion of the GGM-derived geoid to a greater degree (i.e., a higher spatial resolution). Equation (5) can be rewritten as follows:

$$N^{GRA} = N^{GGM+} - \frac{W_0 - U_0}{\gamma_0} \quad (7)$$

Equation (7) presents the so-called gravimetric geoid height according to the constant geopotential W_0 on a global-scale definition. To verify the gravimetric geoid height in Eq. (7), one may use the geometric geoid height N^{GEO}, which can be written as follows:

$$N^{GEO} = h - H^O \quad (8)$$

where h is the ellipsoid height obtained from the GPS/GNSS and H^O is the orthometric height along the plumb line to the geoid. As shown in Fig. 2, in a local

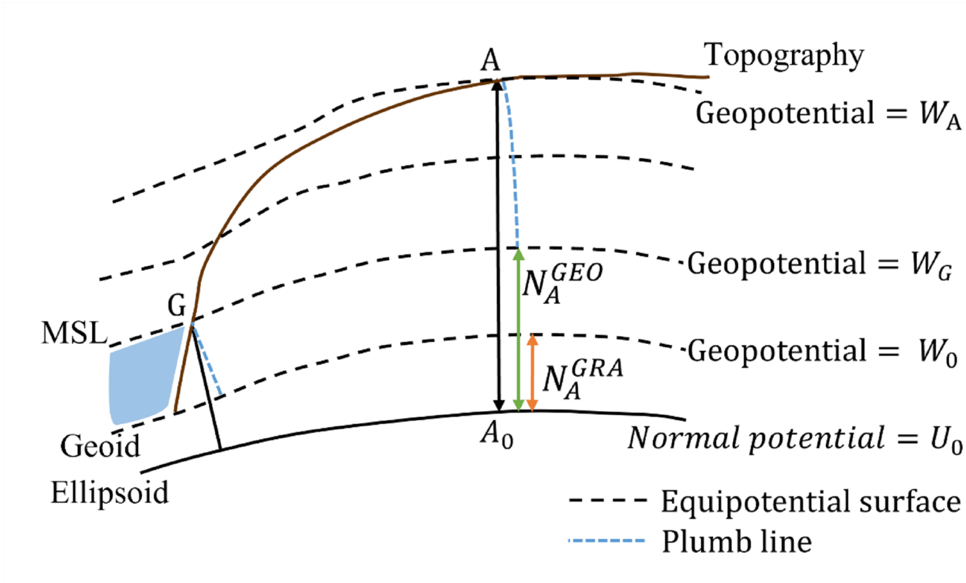

Fig. 2 Geometry between the ellipsoid surface, geoid and mean sea level. Point G serves as the leveling origin with zero orthometric height in the local height system. The gravimetric and geometric geoid heights are defined by aligning the equipotential surface of the geopotential W_0 and W_G, respectively. The normal potential on the ellipsoid surface equals U_0. The ellipsoid height is the distance along the ellipsoid normal direction from A to A_0. The orthometric height in the local height system is defined as the distance along the plumb line from A to the equipotential surface of W_G

height system, one can only measure the height difference from point G to point A by leveling surveys and conducting orthometric correction by using gravity measurements along the leveling route (Guo 2023). Point G serves as the leveling origin with zero orthometric height and is referred to as the MSL at a specific tidal station. In other words, the geometric geoid height derived from the leveling survey aligns the equipotential surface of the geopotential W_G. The difference between the geometric geoid height and the gravimetric geoid height can be written as follows:

$$N^{GEO} = N^{GRA} - \frac{W_G - W_0}{\gamma_0} \tag{9}$$

Considering the variation in the normal gravity γ_0, the second term is approximately a constant in the local area. The geometric geoid heights obtained by leveling surveys based on different MSLs align with different equipotential surfaces, which will result in different mean differences compared to the gravimetric geoid heights.

Furthermore, the gravimetric geoid height N^{GRA} in Eq. (9) can be replaced by that in Eq. (7), which can be rewritten as follows:

$$N^{GEO} = N^{GGM+} - \frac{W_0 - U_0}{\gamma_0} - \frac{W_G - W_0}{\gamma_0} = N^{GGM+} - \frac{W_G - U_0}{\gamma_0} \tag{10}$$

The expression of Eq. (10) is similar to that of Eq. (7). The second term $-\frac{W_G - U_0}{\gamma_0}$ can be regarded as the zero-degree term of the geometric geoid height. As mentioned above, geometric and gravimetric geoid heights were obtained via different methods. Equation (10) can be used to compute the geopotential W_G and can be rewritten as follows:

$$W_G = U_0 + \gamma_0 \cdot \left(N^{GGM+} - N^{GEO}\right) \tag{11}$$

In summary, from a process perspective, the determination of the geopotential W_0 and W_G is crucial for the conversion between global and local vertical datums.

3 Geoid modeling process

In this section, efforts are made to model the portion of the GGM-expanded geoid height mentioned in Eq. (5). The synthesis of the EGM08-derived gravity anomalies and height anomalies was accomplished using the MATLAB-based program 'Graflab' (Buchan, and Janák, 2013). The EGM08-derived gravity anomalies and height anomalies of degree 1800 with a grid spacing of 18 arc seconds, depicted in Fig. 3a and b, were selected as examples to demonstrate the geoid modeling process. The equivalent topography computed from the EGM08-derived gravity anomalies of degree 1800 is depicted in Fig. 4a.

Table 2 summarizes the difference statistics between the EGM08-derived gravity anomalies of degree 1800 and the gravity effects computed using different width settings of the 2D-FFT technique on the equivalent topography. The results showed mean differences, ranging from 1.00 to 1.28 mgal, and the differences in standard deviations ranged from 2.36 to 2.53 mgal. It is assumed that a

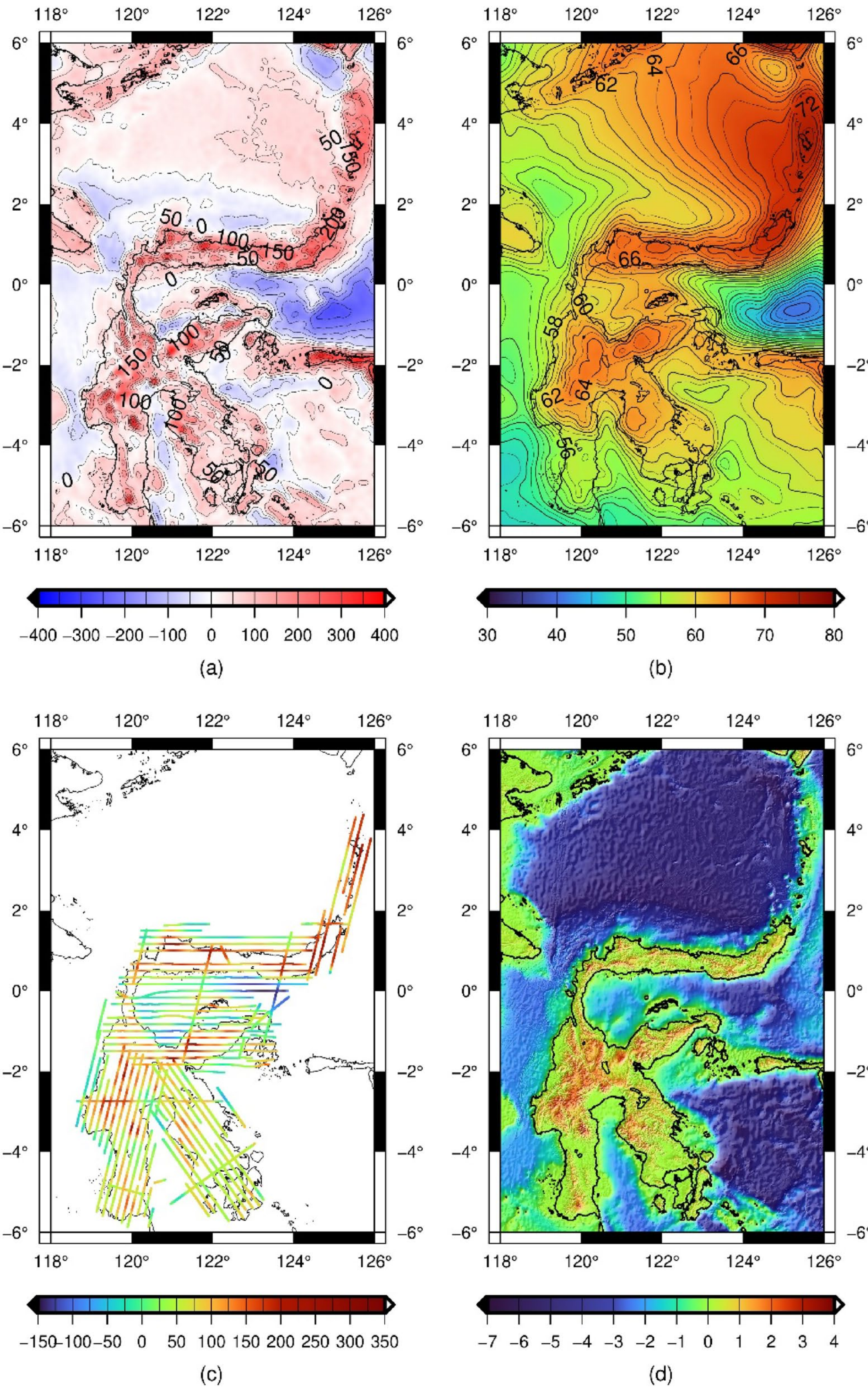

Fig. 3 (**a**) EGM08-derived gravity anomaly (unit: mgal); (**b**) EGM08-derived height anomaly (unit: m); (**c**) airborne gravity anomalies at an average altitude of approximately 3500 m (unit: mgal); and (**d**) Sulawesi's DTM derived from the GEBCO_2022 grid (unit: km). These grids have a grid spacing of 18 arc-seconds

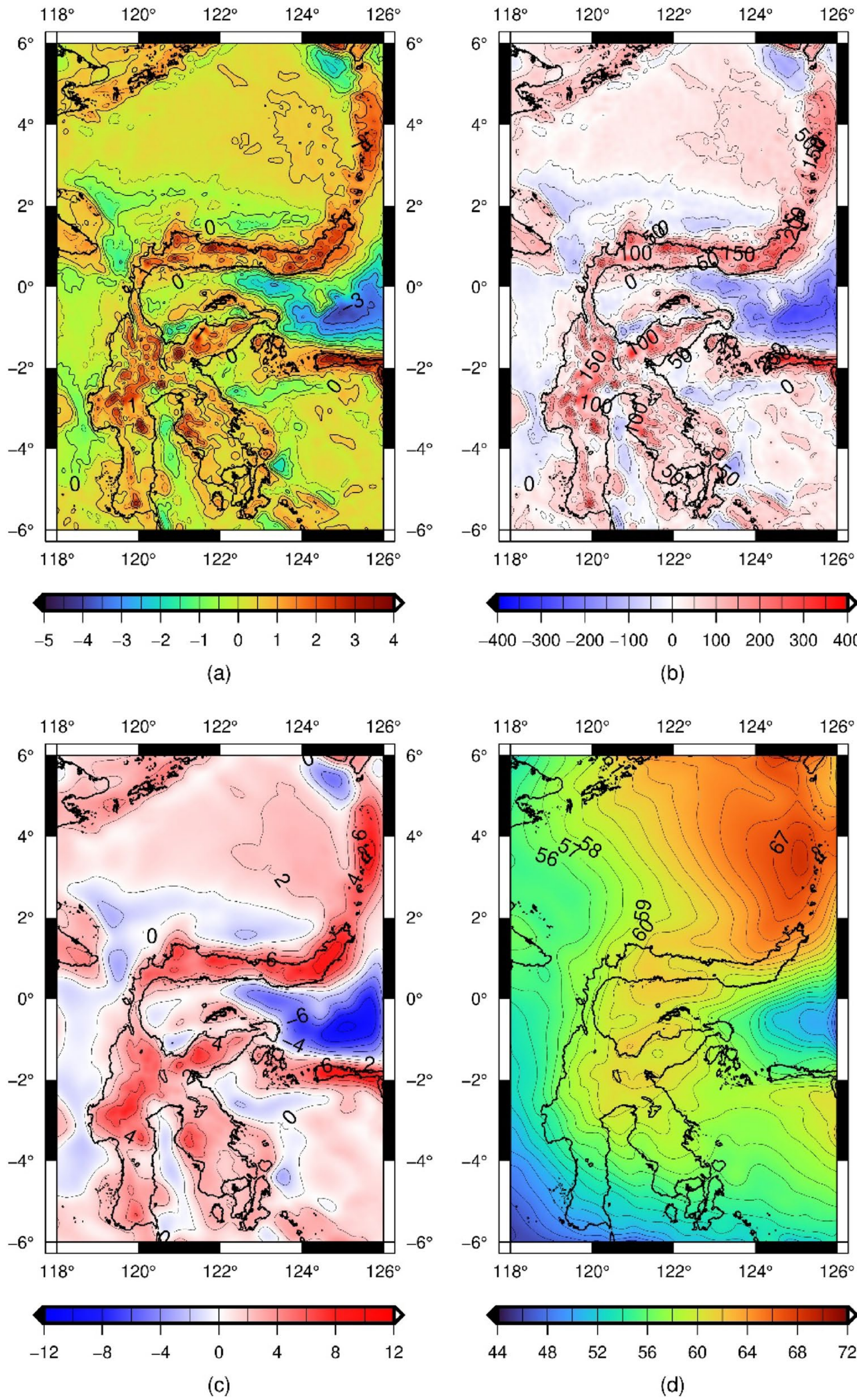

Fig. 4 (**a**) Equivalent topography derived from the EGM08-derived gravity anomaly of degree 1800 (unit: km); (**b**) gravity effects of the equivalent topography (unit: mgal); (**c**) geoid effects of the equivalent topography (unit: m); and (**d)** residual geoid heights (unit: m). These grids have a grid spacing of 18 arc-seconds

Table 2 Difference statistics between the EGM08-derived gravity anomalies of degree 1800 and the gravity effects computed by the 2D-FFT technique and the corresponding equivalent topography (unit: mgal)

FFT	Mean	Maximum	Minimum	Standard deviation	RMS
30	1.00	18.27	−19.19	2.36	2.56
40	1.16	20.58	−17.34	2.45	2.71
50	1.28	22.68	−15.76	2.53	2.84

Bouguer plate with a thickness of 22 m produces a gravity value of approximately 2.46 mgal and its corresponding potential computed by Eq. (3) is $4.48 \times 10^{-4}\, m^2 s^{-2}$. The geoid change due to the potential of the Bouguer plate is approximately 0.05 mm in the equatorial region. For the maximum and minimum values in Table 2, the geoid changes are approximately 0.5 cm. The results show the reliability of geoid modeling by using the 2D-FFT technique on the equivalent topography. After repeated comparative analysis, the 2D-FFT technique with a square of half side length of 40 km was performed on the equivalent topography (Fig. 4a) to obtain the gravity and geoid effects, as depicted in Fig. 4b and c. The residual geoid heights depicted in Fig. 4d were obtained by subtracting the geoid effects of the equivalent topography (Fig. 4c) from the EGM08-derived height anomalies (Fig. 3b).

4 Incorporation with airborne gravity data

From 2008 to 2010, a collaborative effort between the DTU and BIG led to the execution of airborne gravity surveys encompassing the land areas of Sulawesi, Kalimantan, and Papua. The flight lines were spaced approximately 10 nautical miles apart (approximately 16 km), with the aircraft maintaining an average velocity of 150 nautical miles per hour (approximately 77 m/s) (Pahlevi et al. 2015). The cumulative flight time was approximately 750 h. Despite the airborne gravimeter S-99's 1 Hz sampling rate, the spatial resolution of the airborne gravity data obtained after low-pass filtering ranges from 5 to 8 km (Hwang et al. 2006; Shih et al. 2015). Airborne gravity data for Sulawesi were collected at an average altitude of approximately 3500 m.

The ellipsoid heights of the airborne gravity data were adjusted to the orthometric heights by using the EGM08-derived geoid of degree 2160. The normal gravity values were then subtracted from the airborne gravity values to obtain the airborne gravity anomalies. Subsequently, the airborne gravity anomalies were compared with the EGM08-derived gravity anomalies of degree 2160 for each flight line to eliminate evident mismatches and deviations attributed to turbulences (Hwang et al. 2012). The results are depicted in Fig. 3c.

The EGM08-derived gravity anomalies of a specific degree were subtracted from the airborne gravity anomalies to obtain the residual gravity values, which were then used for downward continuation. Notably, the used degree of EGM08 affected the downward-continued residual gravity values and subsequent geoid modeling. To determine the appropriate degree of EGM08 for downward continuation, the analyses of the differences between the airborne gravity anomalies and the EGM08-derived gravity anomalies were conducted at each airborne gravity data point following the methodology proposed by Shih et al. (2015). Table 3 presents the root mean squares (RMS) of the differences between the airborne gravity anomalies and the GGM-derived gravity anomalies at different degrees of the GGMs, such as EGM08, EIGEN 6C4, GECO, XGM2019e, and SGG-UGM-2 (Förste et al. 2014; Shako et al. 2014; Gilardoni et al. 2016; Zingerle et al. 2020; Liang et al. 2018, 2020). The results presented in Fig. 5 revealed that the RMS of the differences exhibited a decreasing trend with increasing degree of EGM08, as do those of the other GGMs. However, beyond 1440 degrees, the reduction in the RMS became less significant. This indicates that employing higher degrees beyond 1440 may not help to further improving the accuracy of downward continuation. In addition, XGM2019e had a better fit to the airborne gravity anomalies than the other GGMs.

The residual gravity values obtained by subtracting the EGM08-derived gravity anomalies of 1800 degrees from the airborne gravity anomalies were gridded onto a 1 arc-minute grid and then continued down to the geoid using the Fourier transform approach as (Buttkus 2000; Hwang et al. 2007, 2014; Hsiao and Hwang 2010).

$$G_0(u,v) = e^{2\pi z\sqrt{u^2+v^2}} F(u,v)\, G_z(u,v) \tag{12}$$

where u and v are spatial frequencies and G_0 and G_z are the Fourier transforms of gravity anomalies at sea level and at the flight altitude, F is a frequency-domain filter. As an alternative to the frequency-domain filtering, one can set $F = 1$ in Eq. (12) and apply a space-domain filter to the unfiltered, downward-continued gravity anomalies. In this study, a space-domain Gaussian filter with a width of 10 km has been used in the Fourier transform approach.

The results are depicted in Fig. 6a, where the dashed line represents the boundary, and values outside the boundary are set to zero. The EGM08-derived gravity anomalies underwent refinement through incorporation of downward-continued residual gravity values, as shown by the refined gravity anomalies in Fig. 6b. Subsequently, the geoid effects computed by using the 2D-FFT technique on the equivalent topography derived from the above-refined gravity anomalies were added to the residual geoid heights (Fig. 4d) to obtain refined geoid heights, as shown in Fig. 6c. Figure 6d shows the differences between the refined geoid heights and the

Table 3 Difference statistics between the airborne gravity anomalies and GGM-derived gravity anomalies at different degrees (unit: mgal)

GGM	Degree	Mean	Maximum	Minimum	Standard deviation	RMS
EGM08	360	−1.91	145.35	−117.57	30.47	30.53
	720	−2.64	98.70	−101.58	20.72	20.89
	1080	−2.77	90.72	−97.08	18.61	18.82
	1440	−2.87	90.63	−92.65	18.30	18.53
	1800	−2.84	90.30	−93.68	18.22	18.44
	2160	−2.79	91.87	−94.59	18.26	18.47
EIGEN −6C4	360	−2.79	91.87	−94.59	18.26	18.47
	720	−1.62	143.30	−116.83	29.98	30.02
	1080	−2.34	100.03	−100.31	20.04	20.17
	1440	−2.47	92.23	−95.90	17.87	18.04
	1800	−2.57	89.85	−91.09	17.56	17.74
	2160	−2.54	89.61	−92.02	17.46	17.65
GECO	360	−1.67	141.23	−113.67	29.63	29.67
	720	−2.39	95.62	−97.67	19.64	19.78
	1080	−2.53	87.64	−93.15	17.37	17.55
	1440	−2.63	83.86	−88.72	17.03	17.23
	1800	−2.59	84.77	−89.75	16.94	17.13
	2160	−2.55	86.26	−90.66	16.99	17.18
XGM 2019e	360	−1.64	129.65	−117.58	28.38	28.43
	720	−2.40	92.43	−100.77	16.40	16.58
	1080	−2.51	89.86	−97.05	13.25	13.49
	1440	−2.59	86.67	−93.70	12.68	12.94
	1800	−2.55	87.75	−94.70	12.66	12.92
	2160	−2.46	90.39	−95.46	12.74	12.98
SGG-UGM-2	360	−1.79	144.73	−115.39	29.75	29.80
	720	−2.62	99.07	−99.88	19.22	19.39
	1080	−2.75	95.79	−96.67	16.85	17.07
	1440	−2.85	88.38	−92.57	16.46	16.71
	1800	−2.82	90.54	−94.64	16.34	16.58
	2160	−2.77	92.28	−96.49	16.36	16.59

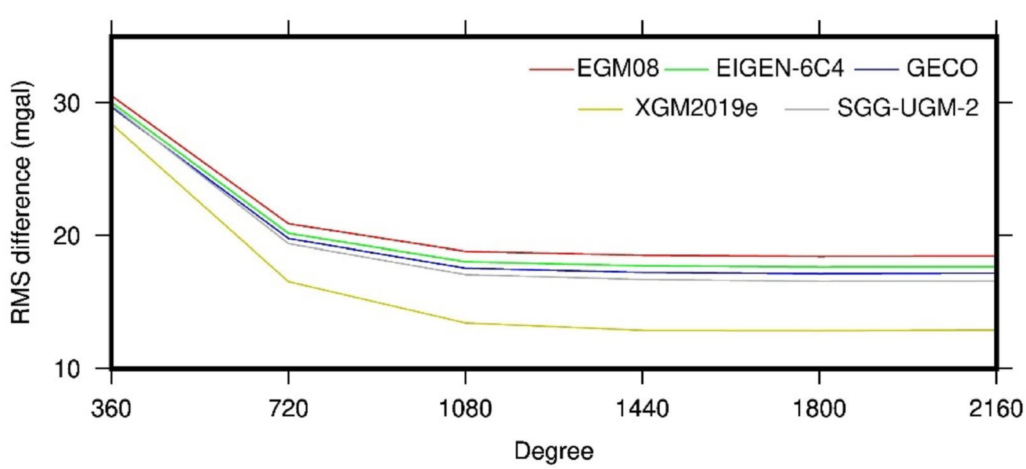

Fig. 5 RMS of the differences between the airborne gravity anomalies and GGM-derived gravity anomalies at different degrees (unit: mgal)

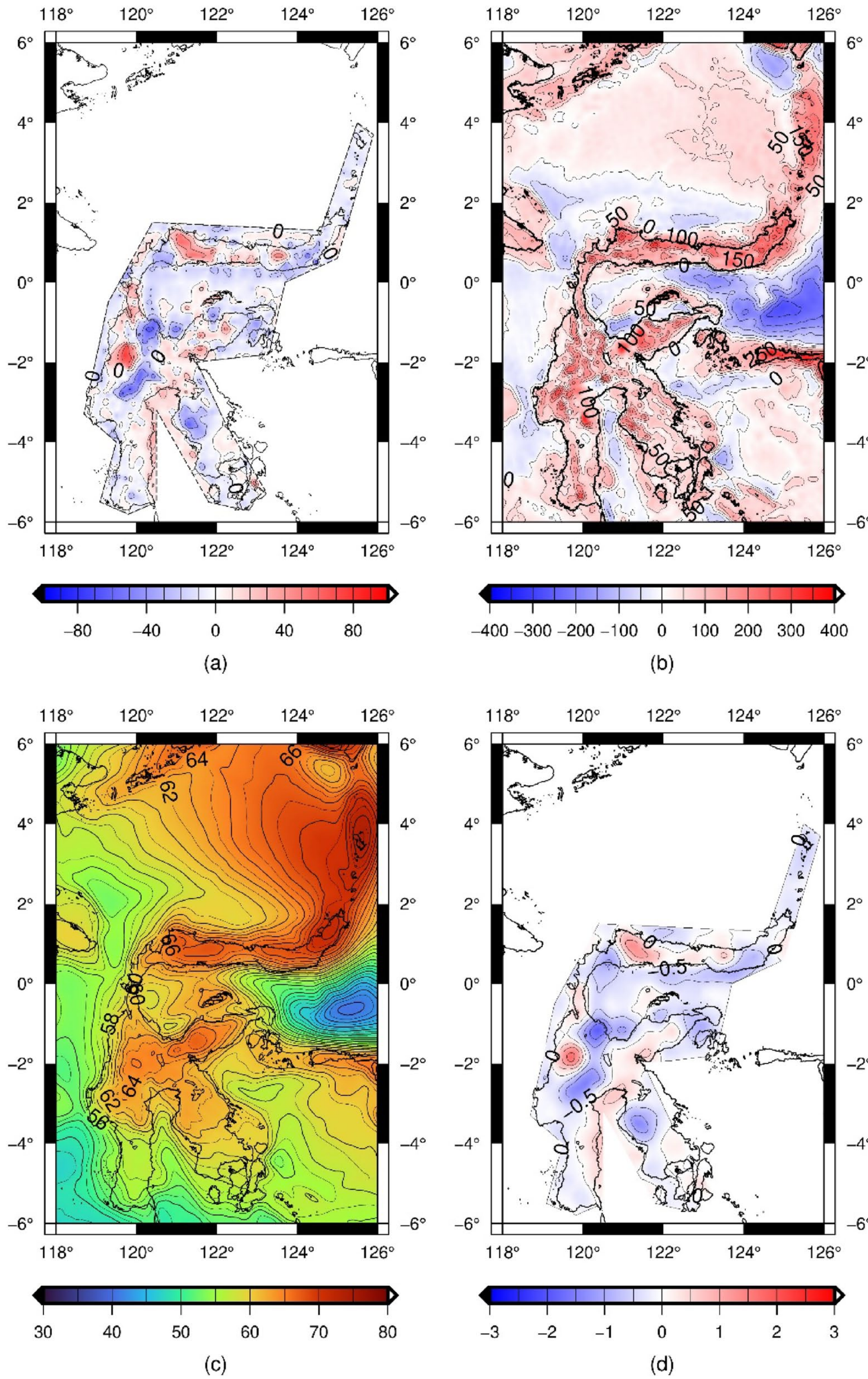

Fig. 6 (**a**) Downward-continued residual gravity data (unit: mgal); (**b**) refined gravity anomalies (unit: mgal); (**c**) refined geoid heights (unit: m); and **(d)** geoid differences (unit: m). The refined model was developed by incorporating the EGM08-derived gravity anomalies of degree 1800 and downward-continued residual gravity. The values outside the boundary (dashed line) are set to zero. The geoid differences show the contribution of downward-continued residual gravity

EGM08-derived geoid heights of degree 1800, in which the differences arose from the contribution of the downward-continued residual gravity values.

5 Incorporation with RTM-derived geoid effects

The GEBCO gridded bathymetry data, known as the GEBCO_2022 Grid, serve as a comprehensive global terrain model encompassing both ocean and land regions. This model furnishes elevation data in meters, featuring a grid spacing of 15 arc-seconds. Additionally, it includes a type identifier (TID) grid, offering insights into the source material characterizing each grid cell in the GEBCO grid. The GEBCO_2022 Grid was developed based on the global topography model from the SRTM. For land areas spanning latitudes between 50° South and 60° North, the GEBCO_2022 Grid incorporates data directly extracted from the SRTM15 + V2.4 dataset (Farr et al. 2007; Tozer et al. 2019). Marine data were further enriched by integrating gridded bathymetric datasets produced by four Seabed 2030 regional centers (https://seabed2030.org/). Notably, the assimilation of heterogeneous data types in generating the GEBCO_2022 Grid assumes that all the data are referenced to the MSL. To optimize the computational efficiency, a resampling process was applied to the original 15 arc-second grid, resulting in a grid spacing of 18 arc-seconds, as illustrated in Fig. 3d. This strategic adjustment aims to alleviate computational loads while maintaining essential geographical information.

A high-pass average filter with a width of 16 km was used on the DTM to obtain the RTM, and the values in the ocean were set to zero. The RTM-derived gravity and geoid effects were computed using the 'TCFOUR' program in 'GRAVSOFT' software with a square of a half-length of 30 km (Forsberg and Tscherning 2008), as depicted in Fig. 7a and b. The RTM-derived gravity effects were added to the refined gravity anomalies (Fig. 5b) to obtain the final gravity anomalies, as depicted in Fig. 7c. The RTM-derived geoid effects were added to the refined geoid heights (Fig. 6c) to obtain the final geoid heights, as depicted in Fig. 7d. The flowchart of the geoid modeling process is depicted in Fig. 8.

6 Validation by geometric geoid heights from GPS/leveling datasets

The geometric geoid heights were obtained from the GPS/leveling dataset. Since the 1980 s, Indonesia has undertaken extensive leveling surveys covering nearly all of its islands. As shown in Fig. 9, the first GPS/leveling dataset contains 9 points using triangles in southwestern Sulawesi, the second GPS/leveling dataset obtained from Pahlevi et al. (2015) contains 44 points using circles, and the third GPS/leveling dataset obtained from Sabri et al. (2021) contains 11 points using squares in southeastern Sulawesi. Note that these legacy datasets, primarily dating back to the 1980 s, lack detailed metadata regarding exact measurement epochs and reference frames. As mentioned above, the orthometric heights obtained from a leveling route refer to an MSL observed at a specific tidal station. For instance, the leveling route in northern Sulawesi started from the Bitung tidal station, while the tidal stations in central Sulawesi were Pare-Pare and Mamuju. In southwestern and southeastern Sulawesi, the tidal stations were Makassar and Kendari, respectively. The locations of these tidal stations are also shown in Fig. 9.

The relationships between the MSLs of these tidal stations remain unclear. The only known information is the leveling routes of the first and third GPS/leveling datasets, which started from the Makassar and Kendari tidal stations, respectively. However, the second GPS/leveling dataset includes several leveling routes referenced to different tidal stations, and it is not clear which points are based on the same tidal station. Furthermore, 9 points with the same position in the first and second datasets are represented by overlapping triangles and circles in Fig. 9. The differences between these points need to be investigated to enhance the understanding of their relationships.

Following the geoid modeling process outlined in Fig. 8, geoid models based on degrees 1440, 1800, and 2160 of EGM08 were produced. The difference statistics between the geometric geoid heights from the three GPS/leveling datasets (D1, D2, and D3) and the modeled geoid heights are summarized in Table 4. For example, the model of EGM08(1440) is the EGM08-derived geoid with a degree of 1440, the model of EGM08(1440 + a) is the geoid model that incorporates airborne gravity data, and the model of EGM08(1440 + a + t) is the geoid model that further incorporates the RTM-derived geoid effects. These notations delineate the progression in model complexity, highlighting the stepwise inclusion of additional data sources and refinements in the geoid modeling process. Particular attention should be given to the changes in the differences in standard deviations, providing valuable insights into the agreement between the geoid models and the GPS/leveling data.

The modeled geoid heights from the EGM08(1440), EGM08(1800), and EGM08(2160) models agree well with the geometric geoid heights from the third GPS/leveling dataset in southeastern Sulawesi, with the differences in standard deviations of approximately 0.06 m (0.055, 0.056 and 0.062 m, respectively, in Table 4). For the first and second GPS/leveling datasets, the differences in standard deviations are approximately 0.18 m (0.186, 0.175, and 0.177 m, respectively, in Table 4) and 0.42 m (0.420, 0.413 and 0.416 m, respectively, in Table 4), respectively. These results indicate that the EGM08-derived geoid model shows better performance in southeastern Sulawesi than

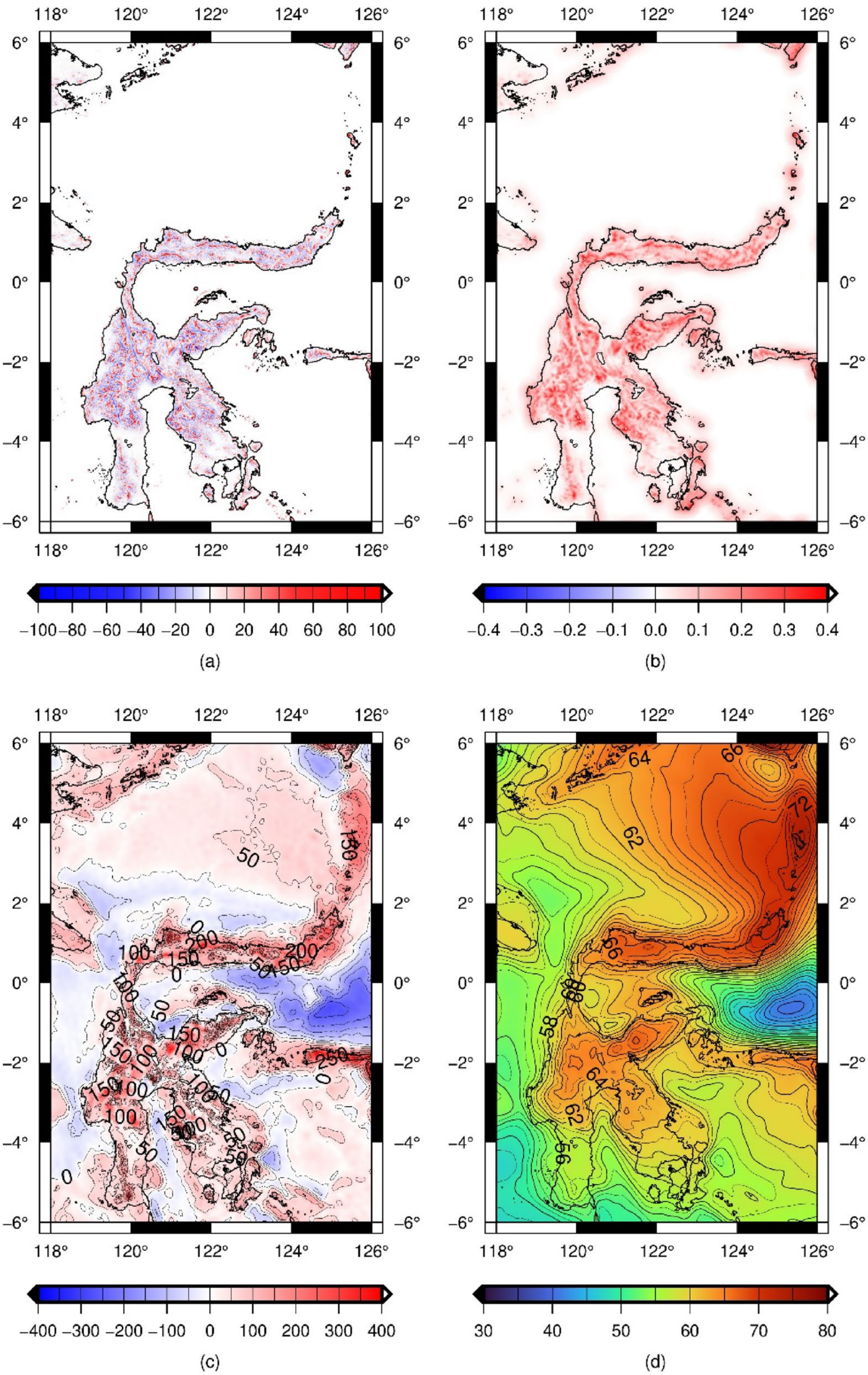

Fig. 7 (**a**) RTM-derived gravity effects (unit: mgal); (**b**) RTM-derived geoid effects (unit: m); (**c**) final gravity anomalies (unit: mgal); and (**d**) final geoid heights (unit: m). The final model was developed by incorporating the EGM08-derived gravity anomalies of degree 1800, downward-continued residual gravity and RTM-derived effects

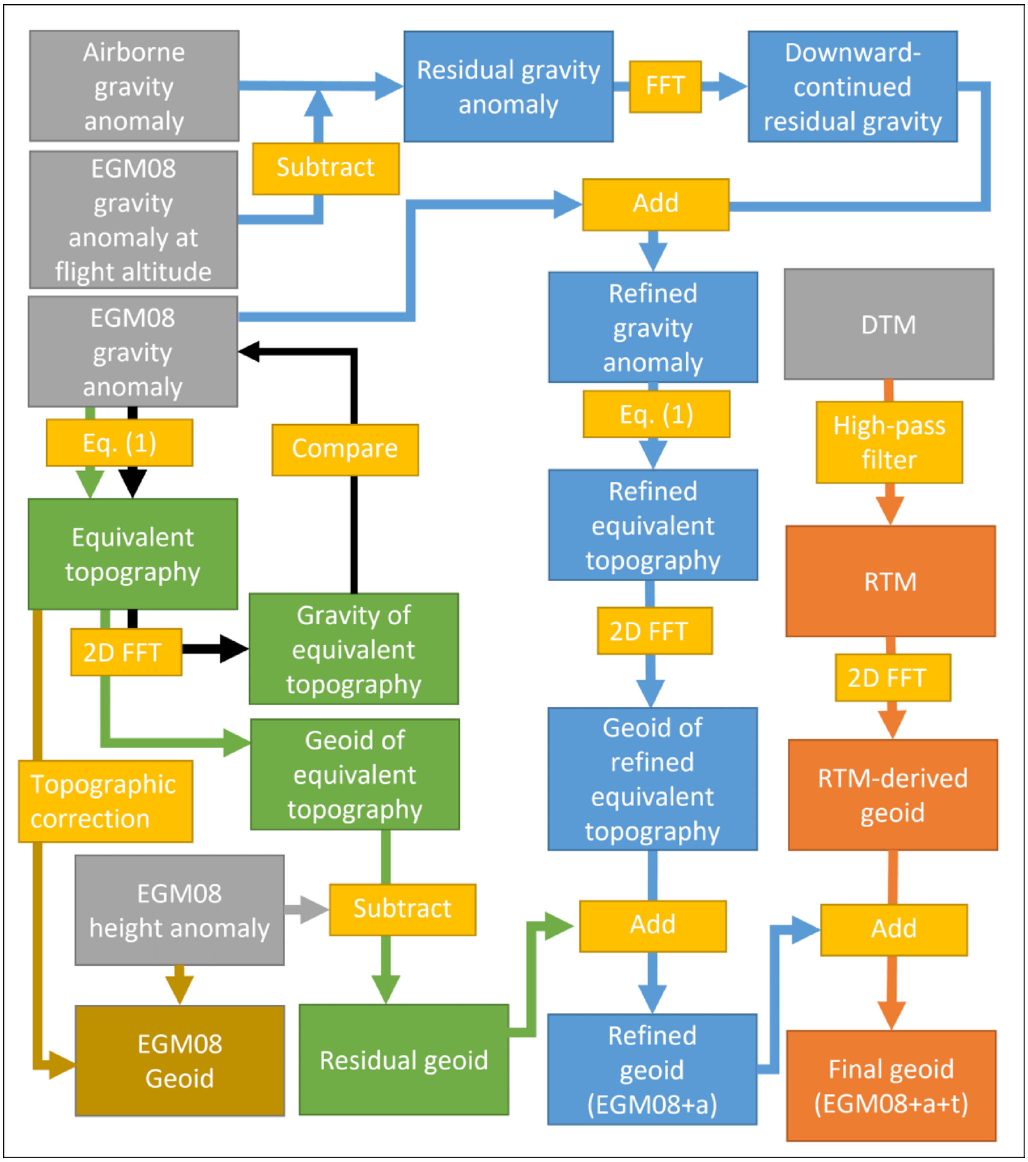

Fig. 8 Chart of the geoid modeling process. The gray blocks represent the datasets that need to be prepared in advance. The yellow blocks are the actions taken. The first loop in black is used to find the half-side length of the square used in the 2D-FFT technique. The sequential processes shown in brown, green, blue and orange are used to calculate the geoid effects from the EGM08, airborne gravity anomaly and RTM data. The outcomes are the models of the EGM08 geoid, the refined geoid (EGM08 + a) and the final geoid (EGM08 + a + t). The model names "+a" and "+t" indicate the incorporation of airborne gravity data and RTM-derived geoid effects, respectively

in other regions. In addition, the results do not show a trend that the higher the degree is, the higher the accuracy, indicating that factors beyond the selected degree will affect the accuracy of the geoid model.

For the three models denoted as "+a", the incorporation of the airborne gravity data results in notable enhancements, as evidenced by a substantial decrease in the differences in standard deviations across all three datasets. Specifically, in the first dataset (D1), the differences in standard deviations decrease significantly from approximately 0.18 m to 0.06 m (0.067, 0.059, 0.062 m, respectively, in Table 4). This improvement underscores the positive impact of incorporating airborne gravity data into the geoid modeling process, contributing to a more accurate and refined geoid model. Comparing the difference statistics obtained from the three models, the degrees 1400, 1800, and 2160 of the EGM08 selected for the downward continuation of the airborne gravity data did not produce significant differences in the geoid modeling (less than 1 cm).

For the three models denoted as " + a + t", the incorporation of the RTM-derived geoid showed slight improvements in the differences in standard deviations across all three datasets (approximately 1 to 2 cm). Notably, the

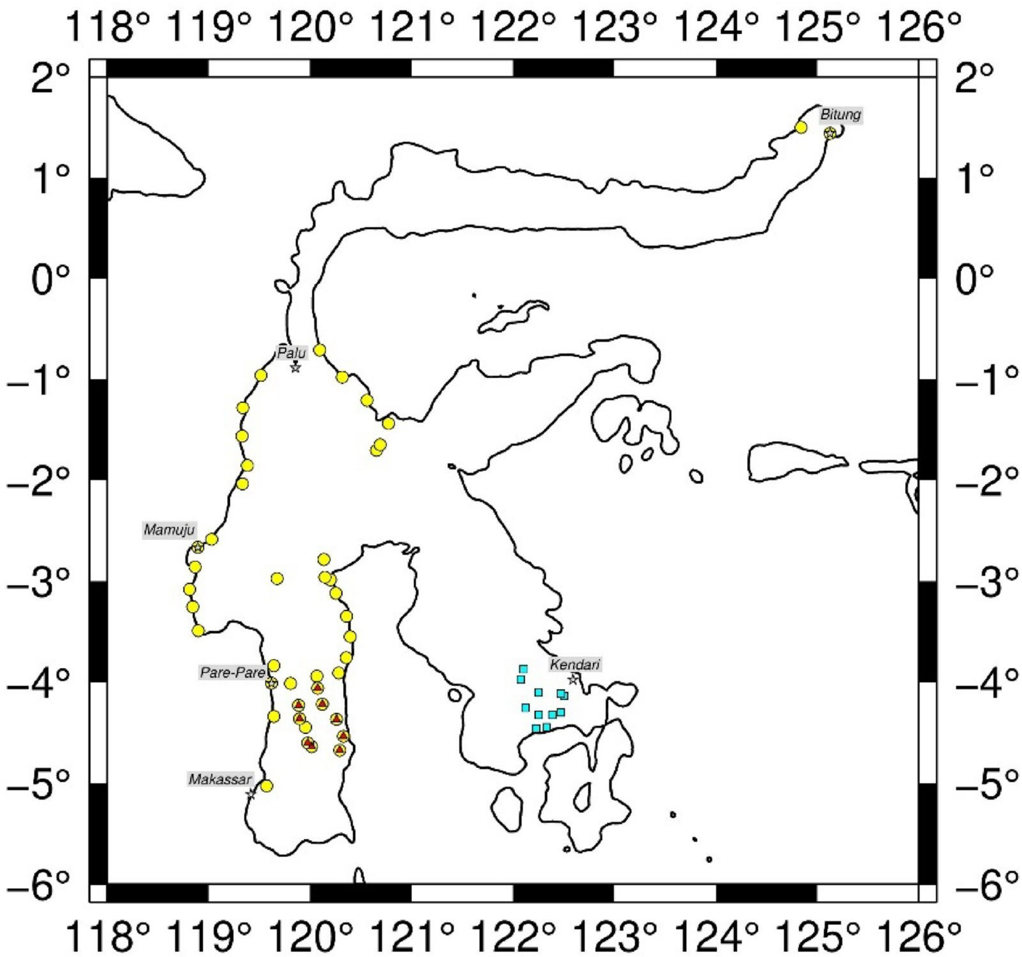

Fig. 9 Three GPS/leveling datasets in Sulawesi (first:; second:; and third:). The text shows the tidal station name and geographical location

EGM08(1800 + a + t) model demonstrated the best fit to the first and third datasets, with differences in standard deviations of 0.052 and 0.037 m, respectively. These results showed that the differences in standard deviations of the first and third datasets are close, yet the discrepancy in the mean of the differences reached approximately 0.24 m (the means of the differences for the first and third datasets were 0.562 and 0.318 m, respectively). This difference is attributed to the different MSLs used in the first and third datasets. Throughout the tests, the second dataset consistently showed the worst results, mainly due to the different MSLs used in this dataset. A detailed examination of the second GPS/leveling dataset is needed, aiming to identify the points from the same tidal station.

6.1 Inspection of GPS/leveling datasets

The difference statistics of the 9 points with the same position in the first and second GPS/leveling datasets showed a mean of 0.285 m and a standard deviation of 0.065 m. Assuming that the accuracy of the geometric geoid heights from the two datasets is comparable, the results showed that the preliminary accuracy estimate of the geometric geoid height was approximately 0.046 m ($0.065/\sqrt{2}$). When assessing the differences between the 9 geometric geoid heights of the first dataset and the geoid heights from the EGM08(1800 + a + t) model, the statistics yielded a mean of 0.561 m and a standard deviation of 0.052 m. The difference statistics between the 9 geometric geoid heights of the second dataset and the geoid heights from the EGM08(1800 + a + t) model yielded a mean of 0.276 m and a standard deviation of 0.051 m. Further statistics can be found in Table 5.

Remarkably, the difference in standard deviations of approximately 0.05 m between the geometric and modeled geoid heights at the 9 points were lower than those obtained by using all points of the second dataset (which yielded a standard deviation of 0.225 m in Table 4). The first GPS/leveling dataset includes newer observations than does the second GPS/leveling dataset. According to the definition of Eq. (7), the mean difference of 0.285 m was the result of changes in the ellipsoid and orthometric heights. This can only be achieved when the increasing rate of the ellipsoid height is greater than that of the

Table 4 Difference statistics between the geometric and modeled geoid heights for the three GPS/leveling datasets (D1, D2 and D3)

Model	Dataset	Mean	Maximum	Minimum	Standard deviation	RMS
EGM08 (1440)	D1	0.773	1.030	0.533	0.186	0.793
	D2	0.460	1.312	−0.720	0.420	0.619
	D3	0.429	0.541	0.346	0.055	0.433
EGM08 (1440 + a)	D1	0.587	0.678	0.507	0.067	0.590
	D2	0.479	1.171	0.167	0.229	0.530
	D3	0.333	0.392	0.253	0.043	0.336
EGM08 (1440 + a + t)	D1	0.562	0.637	0.477	0.061	0.565
	D2	0.430	1.091	0.164	0.222	0.482
	D3	0.312	0.382	0.240	0.040	0.315
EGM08 (1800)	D1	0.775	1.017	0.565	0.175	0.792
	D2	0.464	1.332	−0.664	0.413	0.618
	D3	0.438	0.552	0.353	0.056	0.441
EGM08 (1800 + a)	D1	0.586	0.671	0.519	0.059	0.589
	D2	0.487	1.165	0.185	0.231	0.538
	D3	0.339	0.404	0.259	0.041	0.341
EGM08 (1800 + a + t)	D1	0.562	0.630	0.503	0.052	0.564
	D2	0.438	1.085	0.181	0.225	0.491
	D3	0.318	0.360	0.246	0.037	0.320
EGM08 (2160)	D1	0.766	1.016	0.553	0.177	0.784
	D2	0.466	1.354	−0.649	0.416	0.621
	D3	0.440	0.552	0.338	0.062	0.444
EGM08 (2160 + a)	D1	0.564	0.649	0.477	0.062	0.567
	D2	0.483	1.156	0.157	0.242	0.539
	D3	0.342	0.405	0.252	0.044	0.345
EGM08 (2160 + a + t)	D1	0.540	0.626	0.468	0.058	0.543
	D2	0.435	1.076	0.154	0.238	0.495
	D3	0.321	0.368	0.238	0.041	0.323

sea level rise. Despite this temporal discrepancy, the geometric geoid heights of the 9 points for both the first and second datasets exhibited approximately differences in standard deviations compared to the modeled geoid heights.

Considering the outcomes of the aforementioned tests, the second dataset was divided into five different routes (R1 to R5) based on the geographical location of the point in Sulawesi, as illustrated in Fig. 10 using five different colors. Table 6 provides the difference statistics between the geometric and modeled geoid heights for the five routes. The results demonstrate that the differences in standard deviations ranged from approximately 0.03 to 0.07 m. The EGM08(1800 + a + t) model had a slightly better performance than the EGM08(1440 + a + t) and EGM08(2160 + a + t) models. The mean difference also highlighted the relative relationship of the MSLs used in the five GPS/leveling routes. Since the mean difference between the geometric and modeled geoid heights exceeded 1 m, the MSL of the R5 route was greater than that of the other routes.

7 Estimation of the MSL geopotential

As described in Eq. (9), the difference between the geometric and modeled geoid heights is the zero-degree term of the geometric geoid height. In a small area, the effect of the zero-degree term is approximately constant.

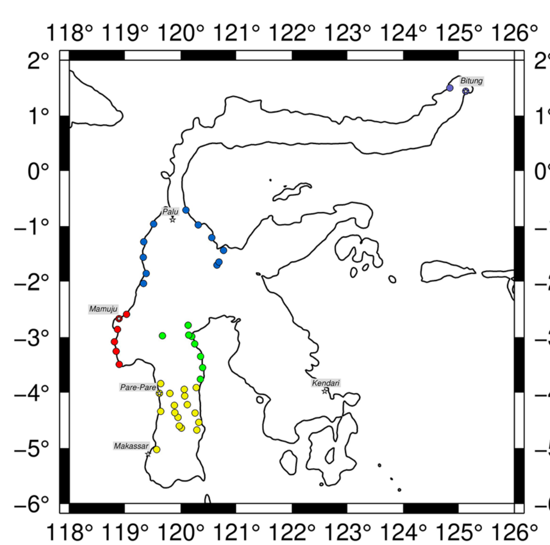

Fig. 10 Five routes divided from the second GPS/leveling dataset (R1: yellow, R2: red, R3: green, R4: blue, and R5: purple)

Table 5 Difference statistics of the 9 points with the same position in the first and second GPS/leveling datasets (unit: m)

Dataset 1		Dataset 2		Modeled geoid heights	Geometric geoid height difference between Datasets 1 and 2	Difference between geometric and modeled geoid heights for Dataset 1	Difference between geometric and modeled geoid heights for Dataset 2
Point name	Geometric geoid height	Point name	Geometric geoid height				
G21	57.423	G722	57.068	56.794	0.355	0.629	0.274
G30	56.893	G723	56.563	56.263	0.330	0.630	0.300
G46	56.844	G724	56.570	56.246	0.274	0.598	0.324
G41	57.288	G725	57.017	56.700	0.271	0.588	0.317
G22	56.980	G727	56.708	56.454	0.272	0.526	0.254
G33	56.987	G728	56.719	56.478	0.268	0.509	0.241
G47	57.051	G730	56.896	56.548	0.155	0.503	0.348
G26	56.800	G731	56.420	56.239	0.380	0.561	0.181
G28	56.950	G732	56.687	56.440	0.263	0.510	0.247
				Mean	0.285	0.561	0.276
				Standard deviation	0.065	0.052	0.051

Table 6 Difference statistics between the geometric and modeled geoid heights for the five routes of the second GPS/leveling dataset (unit: m)

Geoid model	Routes	Mean	Maximum	Minimum	Standard deviation	RMS
EGM08 (1440 + a + t)	R1	0.272	0.368	0.164	0.063	0.279
	R2	0.277	0.309	0.225	0.030	0.279
	R3	0.390	0.473	0.299	0.049	0.393
	R4	0.672	0.753	0.569	0.058	0.674
	R5	1.051	1.091	1.011	0.057	1.052
EGM08 (1800 + a + t)	R1	0.276	0.375	0.181	0.054	0.281
	R2	0.268	0.331	0.198	0.047	0.271
	R3	0.406	0.456	0.374	0.025	0.406
	R4	0.690	0.738	0.633	0.033	0.691
	R5	1.064	1.085	1.043	0.030	1.064
EGM08 (2160 + a + t)	R1	0.256	0.371	0.154	0.056	0.262
	R2	0.285	0.397	0.202	0.067	0.292
	R3	0.397	0.480	0.399	0.047	0.400
	R4	0.703	0.751	0.584	0.047	0.704
	R5	1.067	1.076	1.057	0.013	1.067

Table 7 MSL geopotential Estimation using the points of the first GPS\leveling dataset and the geoid model of EGM08(1800 + a + t)

Model	Point name	Geometric geoid height (m)	Gravimetric geoid height (m)	Geopotential of mean sea level W_G (m^2s^{-2})
EGM08 (1800 + a + t)	G21	57.423	56.794	62636853.848
	G30	56.893	56.263	62636853.840
	G46	56.844	56.246	62636854.147
	G41	57.288	56.700	62636854.251
	G22	56.980	56.454	62636854.857
	G33	56.987	56.478	62636855.017
	G47	57.051	56.548	62636855.076
	G26	56.800	56.239	62636854.510
	G28	56.950	56.440	62636855.013
	Mean			62636854.507
		Standard deviation		0.505

Table 8 MSL geopotential Estimation for the three GPS\leveling datasets (D1, D2 and D3)

Dataset (Route)		Number of Point	Geopotential of mean sea level W_G (m^2s^{-2})	Correction to geometric geoid height $\frac{W_G-U_0}{\gamma_0}$ (m)
D1		9	62636854.507 ± 0.505	−0.562 ± 0.052
D2	R1	17	62636857.299 ± 0.528	−0.276 ± 0.054
	R2	6	62636857.380 ± 0.460	−0.268 ± 0.047
	R3	8	62636856.035 ± 0.244	−0.405 ± 0.025
	R4	11	62636853.252 ± 0.320	−0.690 ± 0.033
	R5	2	62636849.594 ± 0.296	−1.064 ± 0.030
D3		11	62636856.890 ± 0.360	−0.318 ± 0.037

Using Eq. (10), the MSL geopotential estimates using the points of the first GPS\leveling dataset are shown in Table 7. The MSL geopotential of the first GPS\leveling dataset was determined to be 62636854.507 ± 0.505 m^2s^{-2} (approximately ± 5 cm). Similarly, the MSL geopotential estimates of the other GPS\leveling datasets (e.g., the second dataset was separated into five routes from R1 to R5) and the corrections to the geometric geoid heights are summarized in Table 8. These findings underscore the importance of considering MSLs across different GPS/leveling routes, emphasizing the need for consistency in MSLs.

The difference statistics between the corrected geometric geoid heights and the modeled geoid heights of EGM08(1800 + a + t) are summarized in Table 9. The results show a difference in standard deviation of 0.042 m.

8 Impact of the GGM on geoid modeling

When considering the impact of different GGMs on geoid modeling, higher reliability is attributed to GGMs based on the most recent satellite gravity observations. Four GGMs, namely, EIGEN6C4 (Förste et al. 2014; Shako et al. 2014), GECO (Gilardoni et al. 2016), XGM2019e (Zingerle et al. 2020), and SGG-UGM-2 (Liang et al. 2018, 2020), were separately used to replace EGM08 in the geoid modeling process described above. These GGMs are accessible through the International Centre for Global Earth Models (ICGEM) at GFZ and can be obtained via http://icgem.gfz-potsdam.de/home/. In addition, all the GGMs used in this study were based on the zero-tide system. Consequently, the GGMs initially provided in free-tide systems, such as GECO and EIGEN-6C4, were converted to zero-tide systems. The

Table 9 Difference statistics between the corrected geometric and modeled geoid heights (unit: m)

Geoid Model	Dataset (route)		Mean	Maximum	Minimum	Standard deviation	RMS
EGM08	D1		0.000	0.068	−0.059	0.052	0.049
(1800 + a + t)	D2	R1	0.000	0.099	−0.095	0.054	0.052
		R2	0.000	0.063	−0.070	0.047	0.043
		R3	0.001	0.051	−0.031	0.025	0.023
		R4	0.000	0.048	−0.057	0.033	0.031
		R5	0.000	0.021	−0.021	0.030	0.021
	D3		0.000	0.042	−0.072	0.037	0.035
	All		0.000	0.099	−0.095	0.042	0.041

Table 10 Difference statistics between the corrected geometric and modeled geoid heights (unit: m)

Geoid model	GPS/leveling		Mean	Maximum	Minimum	Standard deviation	RMS
EIGEN-6C4	D1		0.847	0.948	0.753	0.062	0.849
(1800 + a + t)	D2	R1	0.880	1.065	0.745	0.087	0.884
		R2	1.000	1.095	0.921	0.059	1.001
		R3	0.915	1.048	0.749	0.106	0.920
		R4	0.949	1.082	0.835	0.065	0.964
		R5	0.954	0.959	0.950	0.006	0.955
	D3		0.984	1.044	0.938	0.039	0.983
	All		0.923	1.095	0.745	0.086	0.927
GECO	D1		0.847	0.945	0.768	0.058	0.849
(1800 + a + t)	D2	R1	0.882	1.088	0.739	0.088	0.886
		R2	0.974	1.014	0.902	0.044	0.975
		R3	0.906	1.022	0.739	0.107	0.911
		R4	0.955	1.069	0.881	0.053	0.957
		R5	0.978	0.985	0.971	0.010	0.978
	D3		0.992	1.049	0.944	0.034	0.993
	All		0.923	1.088	0.739	0.084	0.927
XGM2019e	D1		0.864	0.961	0.756	0.058	0.866
(1800 + a + t)	D2	R1	0.881	1.026	0.734	0.088	0.885
		R2	0.932	0.996	0.856	0.058	0.933
		R3	0.932	1.029	0.723	0.106	0.937
		R4	0.940	1.043	0.769	0.090	0.944
		R5	0.992	1.007	0.977	0.021	0.992
	D3		1.002	1.094	0.890	0.056	1.003
	All		0.924	1.094	0.723	0.089	0.928
SGG-UGM-2	D1		0.860	0.931	0.808	0.046	0.861
(1800 + a + t)	D2	R1	0.889	1.051	0.775	0.072	0.892
		R2	1.018	1.099	0.942	0.055	1.020
		R3	0.924	1.029	0.783	0.079	0.927
		R4	0.965	1.149	0.901	0.069	0.967
		R5	0.870	0.897	0.843	0.038	0.877
	D3		0.999	1.057	0.939	0.036	0.999
	All		0.933	1.149	0.775	0.081	0.936

conversion process involved adjusting the second-degree zonal coefficient, as delineated by Gruber et al. (2014):

$$\bar{C}_{20}^{ZT} = \bar{C}_{20}^{FT} - k_{20}\langle \Delta \bar{C}_{20} \rangle \tag{13}$$

where $\langle \Delta \bar{C}_{20} = \rangle - 1.391412 \times 10^{-8}$ is the average value of the second-degree zonal tidal correction for the sun and moon and k_{20} is the loading Love number for the second-degree zonal coefficient (Amin et al. 2019). This ensures uniformity and consistency in the reference systems across all the GGMs, allowing for standardized

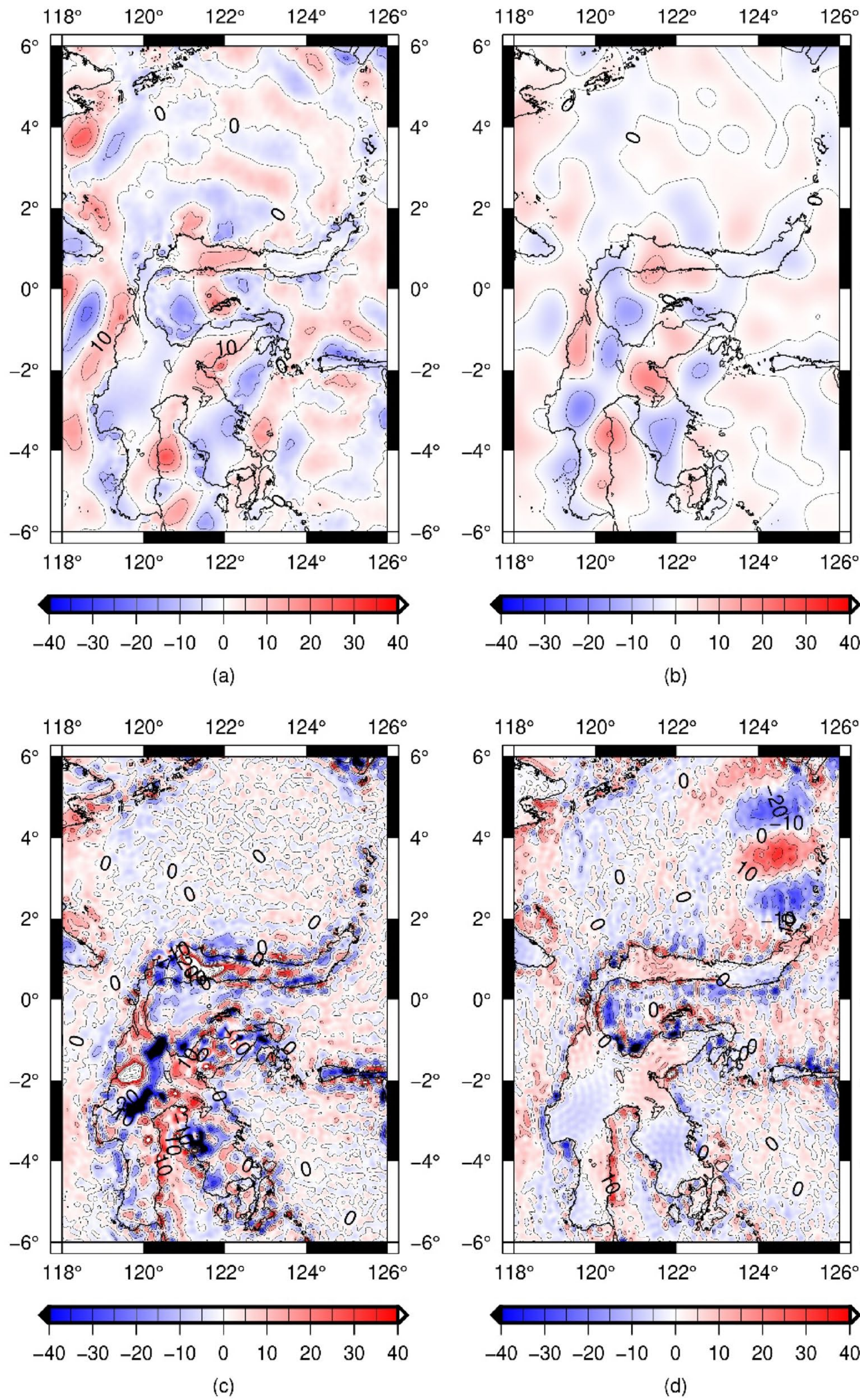

Fig. 11 Differences between the GGM-derived gravity anomalies at 1800: (**a**) EIGEN-6C4 minus EGM08, (**b**) GECO minus EGM08, (**c**) XGM2019e minus EGM08, and (**d**) SGG-UGM-2 minus EGM08

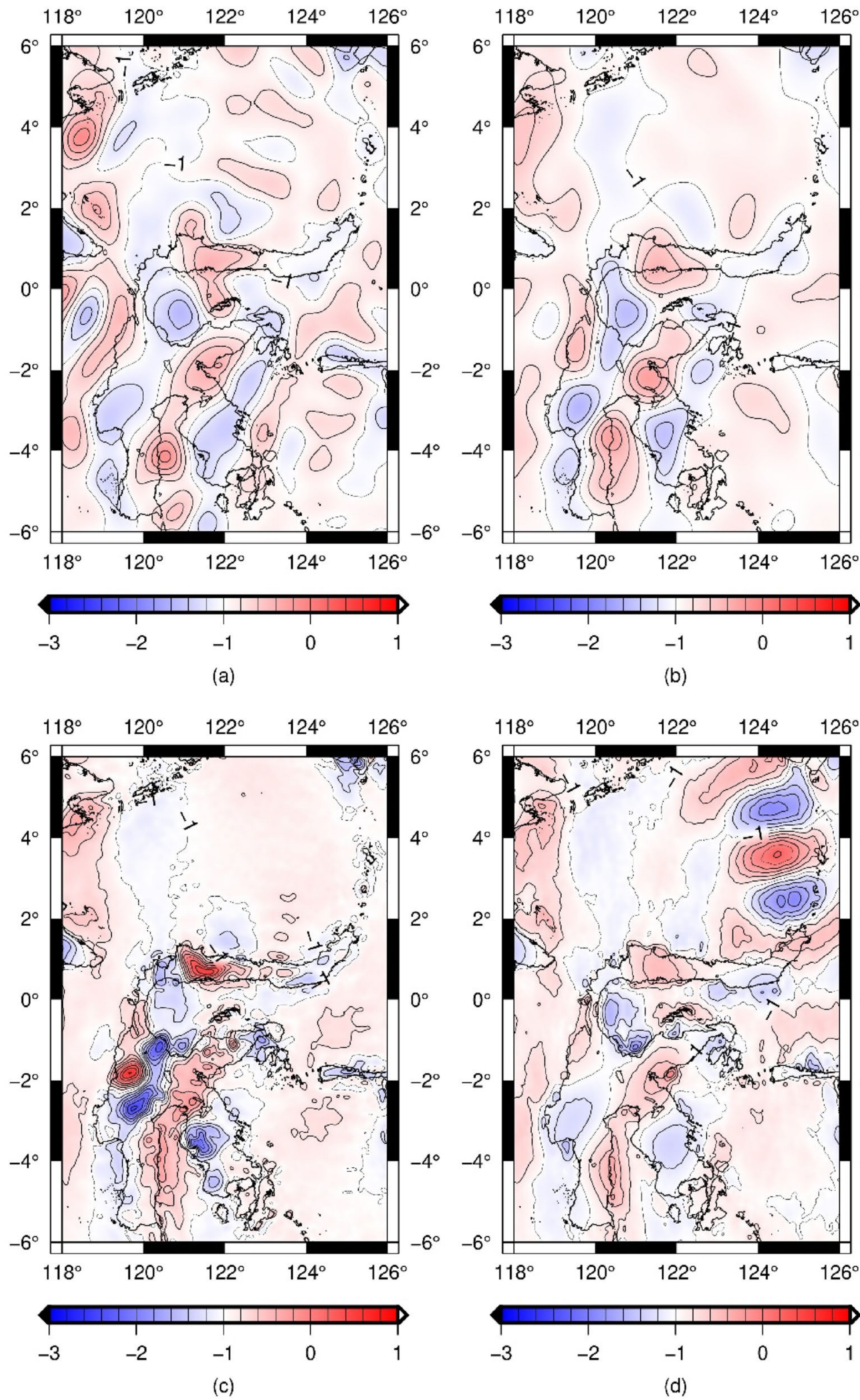

Fig. 12 Differences between the GGM-derived geoid heights at 1800: (**a**) EIGEN-6C4 minus EGM08, (**b**) GECO minus EGM08, (**c**) XGM2019e minus EGM08, and (**d**) SGG-UGM-2 minus EGM08

Table 11 Difference statistics between the GGM-derived gravity anomalies of degree 1800 (unit: mgal)

vs. EGM08	Mean	Maximum	Minimum	Standard deviation	RMS
EIGEN-6C4	0.17	27.01	−21.96	4.99	5.00
GECO	0.15	20.37	−23.10	4.18	4.18
XGM2019e	0.14	98.45	−85.08	9.08	9.09
SGG-UGM-2	0.20	66.54	−74.49	6.24	6.24

Table 12 Difference statistics between the GGM-derived geoid heights of degree 1800 (unit: m)

vs. EGM08	Mean	Maximum	Minimum	Standard deviation	RMS
EIGEN-6C4	−0.935	−0.115	−1.536	0.176	0.952
GECO	−0.936	−0.257	−1.805	0.163	0.951
XGM2019e	−0.935	0.546	−2.466	0.204	0.957
SGG-UGM-2	−0.940	0.173	−1.894	0.184	0.958

Table 13 Datasets used in the development of the GGMs (A: altimetry, S: satellite, G: ground data, and T: topography), obtained from the ICGEM (modified from ICGEM)

GGM	Year	Degree	Data
EGM08	2008	2190	A, G, S(Grace)
EIGEN-6C4	2014	2190	A, G, S(Goce), S(Grace), S(Lageos)
GECO	2015	2190	EGM2008, S(Goce)
XGM2019e	2019	5540	A, G, S(GOCO06s), T
SGG-UGM-2	2020	2190	A, EGM2008, S(Goce), S(Grace)

geoid modeling by the guidelines of International Association of Geodesy (IAG) (Tscherning 1984).

The difference statistics between the corrected geometric geoid heights from the three GPS/leveling datasets and the modeled geoid heights based on different GGMs are summarized in Table 10. Differences in standard deviations larger than 0.06 m can be found for the R1, R3, and R4 routes in the second GPS/leveling dataset. These models showed similar mean differences of 0.92 to 0.93 m and differences in standard deviations of approximately 0.08 to 0.09 m when all three datasets were considered. It should be noted that the differences in the geoid models based on the EGM08 and the other GGMs were not the impact of specific GPS/leveling datasets but the differences between the GGMs. Figures 11 and 12 depict the differences in the gravity anomalies and geoid heights derived from different GGMs at the same degree of 1800. Tables 11 and 12 show the statistics in Figs. 11 and 12, respectively. In Table 11, the differences in means ranged from 0.1 to 0.2 mgal, and the differences in standard deviations ranged from 4 to 9 mgal, showing that there was no systematic bias in the gravity anomalies between these GGMs. However, the statistics in Table 12 show that the mean difference between the geoid heights derived from the other GGMs and the EGM08 was approximately −0.94 m. Thus, the EGM08-derived geoid height was greater than those derived from the other GGMs. This explains the mean difference up to approximately 0.93 m in Table 10.

The differences in the gravity anomalies and geoid heights between the other GGMs and the EGM08 correspond to the different datasets used in the development process, as listed in Table 13. The GECO incorporates data from the Gravity Field and Steady-State Ocean Circulation Explorer (GOCE) mission into the EGM08, which mainly contributes to a moderately low degree of spherical harmonic coefficients of up to 280. It is believed that the GOCE model can provide more information than the EGM08 model in areas where ground gravity data are unavailable, such as Africa, South America, and Antarctica (Gilardoni et al. 2016). In the development of EIGEN-6C4, the satellite and surface datasets mainly contributed spherical harmonic coefficients to degrees up to 370 and were further extended to a degree of 2190 by a block diagonal solution using the DTU10 global gravity anomaly grid (Förste et al. 2014; Shako et al. 2014). Therefore, the major differences between the GECO and the EGM08, the EIGEN-6C4 and the EGM08 models are of low to moderate degrees up to 370, as indicated by the similar differences in distributions shown in Fig. 11a and b. Even disregarding the mean difference, the geoid height differences can be larger than ± 0.5 m. According to the findings of Gilardoni et al. (2016), the standard deviation of the global geoid height difference between the GECO and the EGM08 models is 19.2 cm and can be larger than ± 0.5 m in areas with complex topography (see Fig. 13 in Gilardoni et al. 2016).

In Fig. 11c, the differences between XGM2019e and EGM08 are mainly distributed in the land areas and show more high-frequency changes. Notably, XGM2019e utilizes the GOCO06s satellite-only model, which consists of the GOCE (Brockmann et al. 2019) and GRACE (ITSG-Grace2018s, Kvas et al. 2019) missions; the DTU13 global gravity anomaly grid over the ocean (Andersen et al. 2013); and the EARTH2014 topographic model, which contributes 720 to 5540 degrees (Hirt and Rexer 2015). The airborne gravity datasets used were from Antarctica (Scheinert et al. 2016) and North America (Li et al. 2016) (see Fig. 1 in Zingerle et al. 2020). The EARTH2014 topographic model used in the development of the XGM2019e may be responsible for the high-frequency differences in the land areas. As shown in Fig. 12c, the geoid height differences can be larger than ± 1 m.

Liang et al. (2020) illustrated that the difference between the SGG-UGM-2 and the EGM08 is the datasets of the GOCE and satellite altimetric gravity. In Fig. 11d, large gravity anomaly differences can be found in the offshore areas and the ocean northeast of Sulawesi (see Fig. 8 in Liang et al. 2020). This should be the contribution of the satellite altimetric gravity dataset. As shown in

Fig. 12d, geoid height differences larger than ± 0.5 m are mainly distributed in the nearshore and offshore areas and in the area northeast of Sulawesi.

9 Conclusions

This study presents a significant advancement in geoid modeling for Sulawesi using airborne gravity data, RTM effects, and global gravitational models (GGMs). The combination of these high-resolution datasets and refined methods resulted in a geoid model with improved accuracy, achieving 0.04 to 0.05 m compared to earlier models. These results show the value of airborne gravity surveys and RTM-based refinements in overcoming the challenges posed by complex topography and sparse terrestrial gravity data.

It is clear from this study that there is a critical need for a unified mean sea level (MSL) geopotential to address inconsistencies among diverse GPS/leveling datasets in Sulawesi. Determining a unified geopotential value (W_G) for the various local Mean Sea Levels is a prerequisite for fusing gravimetric and geometric geoid heights. This unification ensures that all dataset refer to a consistent vertical datum, which is essential for developing a high-precision hybrid geoid model that supports direct conversion between local and global height systems. We analyzed various GGMs, such as EGM08, EIGEN-6C4, and XGM2019e, to show the impact of data sources and resolution on geoid accuracy, providing a guidance for future geoid modeling efforts in Sulawesi.

We believe the outcomes of this study have broader implications for sustainable development and disaster management in Indonesia. By enabling accurate spatial referencing, the refined geoid model can support infrastructure planning, resource management, and climate change adaptation. In future studies, we plan to prioritize collecting more GPS/leveling datasets, adopt refined DEMs, and promote regional collaboration to achieve cm-level geoid accuracy in Sulawesi and elsewhere in Indonesia.

Abbreviations

BIG	Badan Informasi Geospasial
DTM	Digital terrain model
DTU	Technical University of Denmark
EGM08	Earth Geopotential Model 2008
FFT	Fast Fourier Transform
GGM	Global gravitational model
GPS	Global Positioning System
GNSS	Global Navigation Satellite System
GOCE	Gravity Field and Steady-State Ocean Circulation Explorer
IAG	International Association of Geodesy
ICGEM	International Centre for Global Earth Models
LSC	Least-squares collocation
MSL	Mean sea level
NCTU	National Chiao Tung University
RCR	Remove-compute-restore
RMS	Root mean squares
RTM	Residual terrain model
SDG	Stainable development goal
SRBF	Spherical radial basis functions
SRTM	Shuttle Radar Topography Mission
TID	Type Identifier

Acknowledgements

The authors would like to thank Ms. Arisauna Maulidyan Pahlevi and Mr. Bagas Triarahmadhana from BIG for their consultation on the airborne gravity data, geometric geoid heights, and relevant datasets in Indonesia.

Author contributions

Hsuan-Chang Shih: conceptualization, data analysis, methodology, software, investigation and validation, writing draft. Leni Sophia Heliani: data curation, methodology, review and editing, discussion. Yu-Shen Hsiao: methodology, review and editing, discussion. Cheinway Hwang: methodology and discussion. Arisauna Maulidyan Pahlevi: data consultation, review and editing.

Funding

This study was funded by the National Taipei University under grants No. 113-NTPU_ORD-F-002, the Ministry of Science and Technology, Taiwan under grants No. 112-2121-M-305-001- and the Ministry of the interior, Taiwan under grants No. 112PL061A.

Data availability

The data that support the findings of this study are available from the corresponding author, Dr. Hsuan-Chang Shih, and requires prior permission from BIG (Indonesia).

Declarations

Ethics approval and consent to participate

Not applicable.

Consent for publication

Not applicable.

Competing interests

The authors declare no competing interests.

Received: 30 July 2025 / Accepted: 25 November 2025
Published online: 02 December 2025

References

Amin H, Sjöberg LE, Bagherbandi M (2019) A global vertical datum defined by the conventional geoid potential and the Earth ellipsoid parameters. J Geod 93:1943–1961. https://doi.org/10.1007/s00190-019-01293-3

Andersen OB, Knudsen P (2019) The DTU17 global marine gravity field: first validation results. In: Mertikas S, Pail R (eds) Fiducial reference measurements for altimetry. International Association of Geodesy Symposia, vol 150. Springer, Cham. https://doi.org/10.1007/1345_2019_65

Andersen OB, Knudsen P, Kenyon S, Factor J, Holmes S (2013) The DTU13 global marine gravity field-first evaluation. Ocean Surf Topogr Sci Team Meet (OSTST), Boulder, Colorado

BIG (2022) Product Information of INAGEOID2020 version 2.0, Sistem Referensi Geospasial Indonesia, Badan Informasi Geospasial, Bogor, Indonesia. https://srgi.big.go.id/page/model-geoid. Accessed 16 May 2024

Brockmann JM, Schubert T, Mayer-Gürr T, Schuh WD (2019) The earth's gravity field as seen by the GOCE satellite: an improved sixth release derived with the time-wise approach (GO_CONS_GCF_2_TIM_R6). https://doi.org/10.5880/ICGEM.2019.003. GFZ Data Services

Buchan B, Janák J (2013) A MATLAB-based graphical user interface program for computing functionals of the geopotential up to ultra-high degrees and orders. Comput Geosci 56:186–196. https://doi.org/10.1016/j.cageo.2013.03.012

Buttkus B (2000) Spectral analysis and filter theory in applied geophysics. Springer, New York

Farr TG, Rosen PA, Caro E, Crippen R, Duren R, Hensley S, Kobrick M, Paller M, Rodriguez E, Roth L, Seal D (2007) The shuttle radar topography mission. Rev Geophys. https://doi.org/10.1029/2005RG000183

Forsberg R (1984) A study of terrain reduction, density anomalies and geophysical inversion methods in gravity field modelling. Reports of the Department of Geodetic Science and Surveying, Ohio State University, p 355

Forsberg R, Tscherning CC (2008) An overview manual for the GRAVSOFT geodetic gravity field modelling programs, Technical University of Denmark (DTU): Kongens Lyngby, Denmark. https://ftp.space.dtu.dk/pub/RF/. Accessed 07 Feb 2024

Förste C, Bruinsma SL, Abrykosov O, Lemoine JM, Marty JC, Flechtner F, Balmino G, Barthelmes F, Biancale R (2014) EIGEN-6C4 the latest combined global gravity field model including GOCE data up to degree and order 2190 of GFZ Potsdam and GRGS Toulouse. https://doi.org/10.5880/icgem.2015.1. GFZ Data Services

GEBCO Bathymetric Compilation Group (2022) GEBCO 2022 Grid. NERC EDS British Oceanographic Data Centre NOC. https://doi.org/10.5285/e0f0bb80-ab44-2739-e053-6c86abc0289c

Gilardoni M, Reguzzoni M, Sampietro D (2016) GECO: a global gravity model by locally combining GOCE data and EGM2008. Stud Geophys Geod 60:228–247. https://doi.org/10.1007/s11200-015-1114-4

Gomez ME, Bagu DR, Cogliano DD, Perdomo RA (2013) Evaluation of terrain corrections through FFT and classical integration in two selected areas of the Andes and their impact on geoidal heights. Bol Ciênc Geod 19:407–419. https://doi.org/10.1590/S1982-21702013000300004

Gruber T, Abrykosov O, Hugentobler U (2014) GOCE high level processing facility-GOCE standards. European GOCE Gravity Consortium 4, GO-TN-HPF-GS-0111

Grzyb M, Krynski J, Mank M (2006) The effect of topography and quality of a digital terrain model on the accuracy of terrain corrections for centimetre quasigeoid modelling. Adv Geodes Geoinform 55(1):23–46

Guo JY (2023) Gravity reduction. In: Guo JY (ed) Physical geodesy: a theoretical introduction. Springer, Cham. https://doi.org/10.1007/978-3-031-23320-3_6

Heiskanen WH, Moritz H (1967) Physical geodesy. W.H. Freeman and Co., San Francisco

Heliani LS, Fukuda Y, Takemoto S (2004) Simulation of the Indonesian land gravity data using a digital terrain model data. Earth Planets Space 56:15–24. https://doi.org/10.1186/BF03352487

Hirt C, Rexer M (2015) Earth2014: 1 arc-min shape, topography, bedrock and ice-sheet models-available as gridded data and degree-10,800 spherical harmonics. Int J Appl Earth Obs Geoinf 39:103–112. https://doi.org/10.1016/j.jag.2015.03.001

Hirt C, Kuhn M, Claessens SJ, Pail R, Seitz K, Gruber T (2014) Study of the Earth's short-scale gravity field using the ERTM2160 gravity model. Comput Geosci 73:71–80. https://doi.org/10.1016/j.cageo.2014.09.00

Hsiao YS, Hwang C (2010) Topography-assisted downward continuation of airborne gravity: an application for geoid determination in Taiwan. Terr Atmos Ocean Sci 21(4):627–637. https://doi.org/10.3319/TAO.2009.07.09.01(T)

Hwang C, Wang CG, Hsiao YS (2003) Terrain correction computation using Gaussian quadrature. Comput Geosci 29(10):1259–1268. https://doi.org/10.1016/j.cageo.2003.08.003

Hwang C, Hsiao YS, Shih HC (2006) Data reduction for scalar airborne gravimetry: theory, computer package and a case study in Taiwan. Comput Geosci 32(10):1573–1584. https://doi.org/10.1016/j.cageo.2006.02.015

Hwang C, Hsiao YS, Shih HC, Yang M, Chen KH, Forsberg R, Olesen AV (2007) Geodetic and geophysical results from a Taiwan airborne gravity survey: data reduction and accuracy assessment. J Geophys Res Solid Earth. https://doi.org/10.1029/2005JB004220

Hwang C, Shih HC, Hsiao YS (2012) Airborne gravity surveys over Taiwan Island and Strait, Kuroshio current and South China sea: comparison of GPS and gravity accuracies at different flight altitudes. Mar Geod 35:287–305. https://doi.org/10.1080/01490419.2011.634962

Hwang C, Hsu HJ, Chang ETY, Featherstone WE, Tenzer R, Lien T, Hsiao YS, Shih HC, Jai PH (2014) New free-air and Bouguer gravity fields of Taiwan from multiple platforms and sensors. Tectonophysics 611:83–93. https://doi.org/10.1016/j.tecto.2013.11.027

Hwang C, Hsu HJ, Featherstone WE, Cheng CC, Yang M, Huang W, Wang CY, Huang JF, Chen KH, Huang CH, Chen H, Su WY (2020a) New gravimetric-only and hybrid geoid models of Taiwan for height modernization, cross-island datum connection and airborne LiDAR mapping. J Geod 94:83. https://doi.org/10.1007/s00190-020-01412-5

Hwang C, Pahlevi AM, Triarahmadhana B, Huda S, Syafarianty AN, Muntaha RIS, Pramono GH (2020b) The progress on recent Indonesia airborne gravity survey. In: 2020 AGU fall meeting, 1–17 December 2020

Hwang C, Shen WB, Li X, Din AHM (2021) Introduction to the special issue on gravity and geoid in the Asia Pacific. Terr Atmos Ocean Sci 32(5):7

Ince ES, Abrykosov O, Förste C, Flechtner F (2020) Forward gravity modelling to augment high-resolution combined gravity field models. Surv Geophys 41:767–804. https://doi.org/10.1007/s10712-020-09590-9

Jekeli C (2000) Heights, the geopotential, and vertical datums. Report 459, dept of civil and environmental engineering and geodetic science. Ohio State Univ, Columbus

Klees R, Tenzer R, Prutkin I, Wittwer T (2008) A data-driven approach to local gravity field modelling using spherical radial basis functions. J Geod 82:457–471. https://doi.org/10.1007/s00190-007-0196-3

Kvas A, Behzadpour S, Ellmer M, Klinger B, Strasser S, Zehentner N, Mayer-Gürr T (2019) ITSG-Grace2018: overview and evaluation of a new GRACE-only gravity field time series. J Geophys Res Solid Earth 124(8):9332–9344. https://doi.org/10.1029/2019JB017415

Li X, Crowley JW, Holmes SA, Wang YM (2016) The contribution of the GRAV-D airborne gravity to geoid determination in the Great Lakes region. Geophys Res Lett 43:4358–4365. https://doi.org/10.1002/2016GL068374

Liang W, Xu X, Li J, Zhu G (2018) The determination of an ultra high gravity field model SGG-UGM-1 by combining EGM2008 gravity anomaly and GOCE observation data. Acta Geod Cartogr Sin 47(4):425–434. https://doi.org/10.11947/j.agcs.2018.20170269

Liang W, Li J, Xu X, Zhang S, Zhao Y (2020) A high-resolution earth's gravity field model SGG-UGM-2 from GOCE, GRACE, satellite altimetry, and EGM2008. Engineering 6(8):860–878. https://doi.org/10.1016/j.eng.2020.05.008

Moritz H (1978) Least-squares collocation. Rev Geophys Space Phys 16(3):421–430

Moritz H (2000) Geodetic reference system 1980. J Geod 74:128–133

Pahlevi AM, Pangastuti D, Sofia N, Kasenda A, Prijatna K (2015) Determination of gravimetric geoid model in Sulawesi Indonesia. In: FIG Working Week 2015, Sofia, Bulgaria, 17–21 May 2015

Pahlevi AM, Sofian I, Pangastuti D, Wijanarto AB (2019) Updating model geoid Indonesia. In: Proceedings of Seminar Nasional Geomatika 2018, Bogor, Indonesia, 5 September 2018. https://doi.org/10.24895/SNG.2018.3-0.1063

Pahlevi A, Syafarianty A, Susilo S, Lumban-Gaol Y, Putra W, Triarahmadhana B, Bramanto B, Muntaha R, Fadhila K, Ladivanov F, Amrossalma H, Islam L, Novianto D, Huda S, Wismadi T, Efendi J, Ramadhan A, Wijaya D, Prijatna K, Pramono G (2024) Geoid undulation model as vertical reference in Indonesia. Sci Data 11(1):822

Pavlis NK, Holmes SA, Kenyon SC, Factor JK (2012) The development and evaluation of the Earth Gravitational Model 2008 (EGM2008). J Geophys Res Solid Earth. https://doi.org/10.1029/2011JB008916

Sabri LM, Sudarsono B, Pahlevi AM (2021) Geoid of South East Sulawesi from airborne gravity using Hotine approach. IOP Conf Ser: Earth Environ Sci 731. https://doi.org/10.1088/1755-1315/731/1/012014

Sánchez L, Čunderlík R, Dayoub N, Mikula K, Minarechová Z, Šíma Z, Vatrt V, Vojtíšková M (2016) A conventional value for the geoid reference potential Wo J Geod 90:815–835. https://doi.org/10.1007/s00190-016-0913-x

Sansò F, Rummel R (1997) Geodetic boundary value problems in view of the one centimeter geoid. Lecture Notes in Earth Sciences, vol 65. Springer

Scheinert M, Ferraccioli F, Schwabe J, Bell R, Studinger M, Damaske D, Jokat W, Aleshkova N, Jordan T, Leitchenkov G, Blankenship D, Damiani T, Young D, Cochran J, Richter T (2016) New Antarctic gravity anomaly grid for enhanced geodetic and geophysical studies in Antarctica. Geophys Res Lett 43(2):600–610. https://doi.org/10.1002/2015GL067439

Shako R, Förste C, Abrykosov O, Bruinsma SL, Marty JC, Lemoine JM, Flechtner F, Neumayer H, Dahle C (2014) EIGEN-6 C: a high-resolution global gravity combination model including GOCE Data. In: Flechtner F, Sneeuw N, Schuh WD (eds) Observation of the system Earth from space – CHAMP, GRACE, GOCE and future missions. Springer, Berlin, pp 155–161. https://doi.org/10.1007/978-3-642-32135-1_20

Shih HC, Hwang C, Barriot JP, Mouyen M, Corréia P, Lequeux D, Sichoix L (2015) High-resolution gravity and geoid models in Tahiti obtained from new airborne and land gravity observations: data fusion by spectral combination geodesy. Earth Planets Space 67:124. https://doi.org/10.1186/s40623-015-0297-9

Sjöberg LE (2003) A computational scheme to model the geoid by the modified Stokes formula without gravity reductions. J Geod 77:423–432. https://doi.org/10.1007/s00190-003-0338-1

Sjöberg LE, Bagherbandi M (2017) Gravity inversion and integration. Springer, Berlin. https://doi.org/10.1007/978-3-319-50298-4

Tozer B, Sandwell DT, Smith WHF, Olson C, Beale JR, Wessel P (2019) Global bathymetry and topography at 15 arc sec: SRTM15+. Earth Space Sci 6(10):1847–1864. https://doi.org/10.1029/2019EA000658

Tscherning CC (1984) The Geodesist's handbook 1984. In: Resolutions adopted by the International Association of Geodesy of the XVIII General Assembly of the International Union of Geodesy and Geophysics, Hamburg, 15–27 August 1983, 58(3). https://office.iag-aig.org/doc/5d7f91ee333a3.pdf. Accessed 16 May 2024

Tscherning CC, Forsberg R, Knudsen P (1992) The GRAVSOFT package for geoid determination. In: Proceedingd of the 1st Continental Workshop on the Geoid in Europe, Prague, May 1992, 327–334

Vaníček P (1994) On the global vertical datum and its role in maritime boundary demarcation. In: Proceedings of International Symposium on Marine Positioning, Hannover, Germany, 19–23 September 1994, 243–250

Vu DT, Bruinsma S, Bonvalot S, Remy D, Vergos GS (2020) A quasigeoid-derived transformation model accounting for land subsidence in the Mekong Delta towards height system unification in Vietnam. Remote Sens 12(5):817. https://doi.org/10.3390/rs12050817

Wang YM, Sánchez L, Ågren J, Huang J, Forsberg R, Abd-Elmotaal HA, Ahlgren K, Barzaghi R, Bašić T, Carrion D, Claessens S, Erol B, Erol S, Filmer M, Grigoriadis VN, Isik MS, Jiang T, Koç Ö, Krcmaric J, Li X, Liu Q, Matsuo K, Natsiopoulos DA, Novák P, Pail R, Pitoňák M, Schmidt M, Varga M, Vergos GS, Véronneau M, Willberg M, Zingerle P (2021) Colorado geoid computation experiment: overview and summary. J Geod 95(12):1–21. https://doi.org/10.1007/s00190-021-01567-9

Yeh TK, Lee TY, Lee I, Shih HC, Chen CH, Yen JY, Ni CF (2025) Combination on GNSS precise point positioning and Insar data fusion to monitor the land subsidence in Taiwan. Geomat Nat Hazards Risk. https://doi.org/10.1080/19475705.2024.2445632

Zingerle P, Pail R, Gruber T, Oikonomidou X (2020) The combined global gravity field model XGM2019e. J Geod 94:66. https://doi.org/10.1007/s00190-020-01398-0

Publisher's note